

DISCOVERY OF LUMINOUS PULSED HARD X-RAY EMISSION FROM ANOMALOUS X-RAY PULSARS 1RXS J1708-4009, 4U 0142+61 AND 1E 2259+586 BY INTEGRAL AND RXTE

L. KUIPER¹, W. HERMSEN^{1,2}, P.R. DEN HARTOG¹ AND W. COLLMAR³

ABSTRACT

Triggered by the earlier surprising detection of pulsed hard X-ray emission from 1E 1841-045, we investigated the time-averaged high-energy spectral characteristics of the established Anomalous X-ray Pulsars, 1RXS J1708-4009, 4U 0142+61, 1E 2259+586 and 1E 1048.1-5937, all with persistent X-ray emission. We report on the discovery of hard spectral tails for energies above 10 keV in the total and pulsed spectra of AXPs 1RXS J1708-4009, 4U 0142+61 and 1E 2259+586 using RXTE PCA (2-60 keV) / HEXTE (15-250 keV) data and INTEGRAL IBIS ISGRI (20-300 keV) data. 1E 1048.1-5937 appeared to be too weak to be detected with the presently available exposure. Furthermore, improved spectral information for 1E 1841-045 is presented. The pulsed and total spectra measured above 10 keV have power-law shapes and there is so far no significant evidence for spectral breaks or bends up to ~ 150 keV. The pulsed spectra above 10 keV are exceptionally hard with indices measured for four AXPs approximately in the range $-1.0 - 1.0$. The indices measured for these pulsed spectra below 10 keV were in the range $2.0 - 4.3$, indicating the very drastic spectral changes in a narrow energy interval around 10 keV, where clear minima are found in luminosity. The best fit power-law models to the total spectra between ~ 10 and 150 keV are significantly softer, with indices measured for three AXPs, 1E 1841-045, 1RXS J1708-4009 and 4U 0142+61 in the range $1.0 - 1.4$. For the latter AXPs the pulsed fractions are consistent with 100% around 100 keV, but are different at 10 keV: 4U 0142+61 $\sim 10\%$, 1E 1841-045 $\sim 25\%$, and 1RXS J1708-4009 consistent with 100%. The luminosities of these total and pulsed spectral tails (10-150 keV) largely exceed the total available spin-down powers by factors ranging from ~ 100 to ~ 600 . This shows that also these new hard-X-ray components cannot be powered by rotational energy loss. We reanalyzed archival CGRO COMPTEL (0.75-30 MeV) data to search for signatures from our set of AXPs. No detections can be claimed, but the obtained upper-limits to soft gamma-ray emission in this MeV range indicates for 1RXS J1708-4009, 4U 0142+61 and 1E 1841-045 that strong breaks or bends must occur somewhere between ~ 150 keV and 750 keV. We discuss predictions from first attempts to model our hard X-ray / soft gamma-ray spectra in the context of the magnetar model. Our spectral results cannot yet discriminate between the different proposed scenarios. Particularly, more constraining information is required on the detailed shape of the spectra between ~ 150 keV (our highest data points from INTEGRAL) and 750 keV, from where we report the COMPTEL upper limits.

Subject headings: pulsars: individual (1RXS J1708-4009; 4U 0142+61; 1E 2259+586; 1E 1048.1-5937; 1E 1841-045), X-rays: stars

1. INTRODUCTION

Anomalous X-ray pulsars (AXP) belong to a class of rare objects closely concentrated along the Galactic plane, known to emit pulsed X-rays for energies below 10 keV with pulse periods in the range $\sim 6 - 12$ s and characteristic spin-down time scales of $\sim 10^3 - 10^5$ year. Two, probably three, members of this class are embedded in a shell-like supernova remnant (SNR; see e.g. Gregory & Fahlman 1980; Kriss et al. 1985). The fact that the observed X-ray luminosity is much larger than the spin-down power excludes an interpretation in which the (pulsed) X-ray emission originates from a spin-down powered pulsar. On the other hand, the steady spin-down without a doppler modulated signature and the lack of bright optical counterparts make an X-ray binary interpretation, in which mass transfer (accretion) powers the high-energy emission of the system, very unlikely (see Mereghetti et al. 2002, for a review on AXPs). Currently, models based on the decay of very strong magnetic fields ($10^{14} - 10^{15}$ Gauß) - so called “magnetar” models (Thompson & Duncan 1996) - seem to explain the observed high-energy characteristics of AXPs at a satisfactory level. For instance, the recently detected bursts from the AXPs 1E 1048.1-5937 (Gavril et al. 2002b) and 1E 2259+586 (Kaspi et al. 2003) mimic the bursting behaviour of Soft Gamma-ray Repeaters (SGR) for which the magnetar model was initially developed. Also, the “glitch” phenomenon detected in the spin-down of some AXP members fits in this model (Kaspi et al. 2000, 2003; Morii et

al. 2005). These properties provide strong evidence that both AXPs and SGRs are members of the same source class.

The X-ray spectra of AXPs in the 0.5-10 keV band are very soft and can best be described by a black body plus a power-law model. The softness of the spectra below 10 keV (power-law indices $2 < \Gamma < 4$, with $F_\gamma \propto E^{-\Gamma}$) predicts non-detections for energies above 10 keV and thus explains the initial ignorance for studying the spectral properties of AXPs at energies above 10 keV.

It was a great surprise that the high-resolution imaging instrument IBIS/ISGRI aboard ESA’s INTEGRAL satellite measured hard X-rays from the direction of three AXPs. Firstly, Molkov et al. (2004) reported the discovery of an INTEGRAL source at the position of AXP 1E 1841-045 in SNR Kes 73 for energies up to 120 keV (60–120 keV: 7.5σ). This was followed up by Kuiper et al. (2004), who analysed archival RXTE PCA and HEXTE data from monitoring observations spread over four years, to prove that the hard X-ray emission comes from the AXP and not from the SNR. They discovered non-thermal pulsed hard X-ray / soft γ -ray emission up to ~ 150 keV with a spectrum with power-law photon index of ~ 0.94 .

Secondly, Revnivtsev et al. (2004) published the INTEGRAL detection (18–60 keV: 6.5σ) of AXP 1RXS J170849.0-400910 (we use throughout this paper: 1RXS J1708-4009), also in a spatial analysis of ISGRI data. Similarly, den Hartog et al. (2004) reported the detection of AXP 4U 0142+61 (50–100

keV: 6.1σ) which exhibited a very hard total spectrum above 20 keV. These three AXPs reach about the same flux level around 100 keV.

In this paper we present the results from follow-up studies using archival RXTE PCA and HEXTE data of 1RXS J1708-4009, 4U 0142+61, 1E 2259+586 and 1E 1048.1-5937 aimed at studying their timing and spectral characteristics above 10 keV. We also revisit the pulsed high-energy emission properties of 1E 1841-045 above 10 keV using more RXTE PCA data and applying now more-optimized event selection criteria. Furthermore, we explored the INTEGRAL database using both public, private and core program data to derive the total X-ray emission spectra of the five AXPs mentioned above, and reanalyze archival data from COMPTEL (Schönfelder et al. 1993), delivering constraining upper limits in the soft gamma-ray band 0.75-30 MeV. Finally, initial results will be shown from IBIS ISGRI timing analysis studies of 1RXS J1708-4009 and 1E 1841-045.

2. INSTRUMENTS AND OBSERVATIONS

2.1. Rossi X-ray Timing Explorer

In this study extensive use is made of data from monitoring observations of AXPs with the two non-imaging X-ray instruments aboard RXTE, the Proportional Counter Array (PCA; 2-60 keV) and the High Energy X-ray Timing Experiment (HEXTE; 15-250 keV). The PCA (Jahoda et al. 1996) consists of five collimated xenon proportional counter units (PCUs) with a total effective area of $\sim 6500\text{ cm}^2$ over a $\sim 1^\circ$ (FWHM) field of view. Each PCU has a front Propane anti-coincidence layer and three Xenon layers which provide the basic scientific data, and is sensitive to photons with energies in the range 2-60 keV. The energy resolution is about 18% at 6 keV.

The HEXTE instrument (Rothschild et al. 1998) consists of two independent detector clusters, each containing four Na(Tl)/CsI(Na) scintillation detectors. The HEXTE detectors are mechanically collimated to a $\sim 1^\circ$ (FWHM) field of view and cover the 15-250 keV energy range with an energy resolution of $\sim 15\%$ at 60 keV. The collecting area is 1400 cm^2 taking into account the loss of the spectral capabilities of one of the detectors. The maximum time resolution of the tagged events is $7.6\mu\text{s}$. In its default operation mode the field of view of each cluster is switched on and off source to provide instantaneous background measurements. Due to the co-alignment of HEXTE and the PCA, they simultaneously observe the sources. Table 1 lists the publicly available RXTE observations used in this study. In the fourth column the PCU unit-2 screened (see Sect 3.1) exposure is given. A typical observation consists of several sub-observations spaced more or less uniformly between the start and end date of the observation.

2.2. INTEGRAL

The INTEGRAL spacecraft (Winkler et al. 2003), launched 17 October 2002, carries two main γ -ray instruments: a high-angular-resolution imager IBIS (Ubertini et al. 2003) and a high-energy-resolution spectrometer SPI (Vedrenne et al. 2003). These instruments make use of coded aperture masks enabling image reconstruction in the hard X-ray/soft γ -ray band.

In our study, guided by sensitivity considerations, we only used data recorded by the INTEGRAL Soft Gamma-Ray Imager ISGRI (Lebrun et al. 2003), the upper detector system of IBIS, sensitive to photons with energies in the range $\sim 20\text{ keV} - 1\text{ MeV}$. With an angular resolution of about $12'$ and a source

TABLE 1

LIST OF RXTE OBSERVATIONS OF 1RXS J1708-4009, 4U 0142+61, 1E 2259+586 AND 1E 1048.1-5937 USED IN THIS STUDY. FOR OBSERVATIONS USED IN THE REANALYSIS OF 1E 1841-045 SEE SECT. 8.1 AND KUIPER ET AL. (2004).

Obs. id.	Begin/End Date (dd/mm/yyyy)		Exp. [†] (ks)
<i>1RXS J1708-4009</i>			
30125	12-01-1998	08-01-1999	59.896
40083	06-02-1999	11-03-2000	52.568
50082	21-04-2000	12-05-2001	34.576
60412	20-05-2001	23-05-2001	9.928
60069	06-05-2001	20-02-2002	24.544
70094	02-04-2002	20-03-2003	55.600
80098	16-04-2003	26-10-2003	73.368
All	12-01-1998	26-10-2003	310.480
<i>4U 0142+61</i>			
10193	28-03-1996	29-03-1996	37.728
10185	28-03-1996	28-03-1996	16.288
20146	24-11-1996	13-12-1997	10.600
30110	21-03-1998	21-03-1998	15.408
50082	07-03-2000	10-02-2001	34.240
60069	18-03-2001	08-01-2002	42.272
70094	06-03-2002	26-12-2002	82.464
80098	28-03-2003	18-09-2003	38.664
80099	03-09-2003	09-09-2003	29.216
All	28-03-1996	18-09-2003	306.880
<i>1E 2259+586</i>			
10192	29-09-1996	30-09-1996	75.936
20145	25-02-1997	25-03-1997	101.024
20146	24-11-1996	13-12-1997	9.784
30126	13-08-1998	02-12-1998	103.136
40083	17-01-1999	01-03-2001	48.344
40082	26-01-2000	27-03-2000	87.120
50082	10-03-2000	02-03-2001	50.280
60069	16-04-2001	07-02-2002	49.592
70094	22-03-2002	15-02-2003	149.840
80098	15-03-2003	28-10-2003	71.960
All	29-09-1996	28-10-2003	747.016
<i>1E 1048.1-5937</i>			
10192	29-07-1996	30-07-1996	72.344
20146	24-11-1996	13-12-1997	12.616
40083	23-01-1999	10-02-2000	49.184
50082	11-03-2000	09-02-2001	40.992
60069	06-03-2001	25-02-2002	139.776
70094	12-03-2002	25-02-2003	133.224
80098	12-03-2003	24-02-2004	136.376
All	29-07-1996	24-02-2004	584.512

[†]PCU-2 exposure after screening

location accuracy of better than $1'$ (for a $> 10\sigma$ source) this instrument is able to locate and separate high-energy sources in crowded fields within its $19^\circ \times 19^\circ$ field of view (50% partially coded) with an unprecedented sensitivity ($\sim 960\text{ cm}^2$ at 50 keV). Its energy resolution of about 7% at 100 keV is amply sufficient to determine the (continuum) spectral properties of hard X-ray sources in the $\sim 20 - 300\text{ keV}$ energy band.

The timing accuracy of the ISGRI time stamps recorded on board is about $61\mu\text{s}$. The time alignment between INTEGRAL and RXTE is better than $\sim 25\mu\text{s}$, verified using data from simultaneous RXTE and INTEGRAL observations of the accretion-powered millisecond pulsar IGR J00291+5934 (Falanga et al. 2005); for a calibration on the Crab pulsar, see also Kuiper et al. (2003). Given the fact that the accuracy of the RXTE clock in absolute time is about $2\mu\text{s}$ (Rots et al. 2004), this implies that the INTEGRAL absolute timing is better than $\sim 27\mu\text{s}$. Data from regular INTEGRAL Crab monitoring observations show

TABLE 2

LIST OF INTEGRAL OBSERVATIONS, SORTED ON INTEGRAL ORBITAL REVOLUTIONS (REV.), OF THE AXPs STUDIED IN THIS WORK. FOR MORE DETAILS ON THE EXECUTED INTEGRAL OBSERVATIONS, SEE [HTTP://INTEGRAL.ESAC.ESA.INT/](http://integral.esac.esa.int/)

Rev. begin	Rev. end	Begin/End Date (dd/mm/yyyy)	
Imaging analysis			
<i>1RXS J1708 - 4009</i>			
36	106	29-01-2003	29-08-2003
<i>4U 0142+61</i>			
47	92	03-03-2003	16-07-2003
142	148	12-12-2003	01-01-2004
153	153	14-01-2004	15-01-2004
161	162	07-02-2004	12-02-2004
177	234	26-03-2004	12-09-2004
238	238	25-09-2004	27-09-2004
261	266	02-12-2004	19-12-2004
268	269	24-12-2004	28-12-2004
<i>1E 1841-045</i>			
49	253	10-03-2003	08-11-2004
<i>1E 2259+586</i>			
142	148	12-12-2003	01-01-2004
161	162	07-02-2004	12-02-2004
<i>1E 1048.1 - 5937</i>			
36	217	29-01-2003	24-07-2004
Timing analysis			
<i>1RXS J1708 - 4009</i>			
36	120	29-01-2003	10-10-2003
<i>1E 1841-045</i>			
49	123	10-03-2003	18-10-2003

that the clock behaviour is stable, making deep timing studies of weak pulsars possible.

In its default operation mode INTEGRAL observes the sky in a dither pattern with 2° steps, which could be rectangular e.g. a 5×5 dither pattern with 25 grid points, or hexagonal with 7 grid points (target in the middle). Typical integration times for each grid point (pointing/sub-observation) are in the range 1800 - 3600 seconds. This strategy drives the structure of the INTEGRAL data archive which is organised in so-called science windows (Scw) per INTEGRAL orbital revolution (lasting for about 3 days) containing the data from all instruments for a given pointing. Most of the INTEGRAL data reduction in this study was performed with the Offline Scientific Analysis (OSA) version 4.1 distributed by the INTEGRAL Science Data Centre (ISDC; see e.g. Courvoisier et al. 2003).

Table 2 lists the INTEGRAL orbital revolution identifiers with corresponding start/end dates of the observations used in the imaging/spectral analyses and timing analyses of the selected sample of persistent AXPs.

2.3. COMPTEL

The Compton telescope COMPTEL aboard the Compton Gamma-Ray Observatory (CGRO, 1991 – 2000) was sensitive to γ -ray photons between 0.75 and 30 MeV, thereby covering the harder γ -ray band adjacent to the INTEGRAL one. The very hard spectra that we measured with IBIS ISGRI for some AXPs warranted us to revisit the COMPTEL data archive to search for signals from AXPs. COMPTEL has an energy-dependent energy and angular resolution of 5% – 8% (FWHM) and 1.7° – 4.4° (FWHM), respectively, and a wide circular field of view covering ~ 1 steradian. Imaging in its large field of view is pos-

sible with a location accuracy (flux dependent) of the order of 0.5° – 2° . For details on the experiment see Schönfelder et al. (1993).

3. ANALYSIS METHODS

3.1. RXTE PCA/HEXTE timing

The PCA data from the observations listed in Table 1 have all been collected in *Goodxenon* or *GoodxenonwithPropane* mode allowing high-time-resolution ($0.9\mu\text{s}$) studies in 256 spectral channels. Because we are mainly interested in the medium/hard (> 2 keV) X-ray timing properties of the selected sample of AXPs, we ignored the events triggered in the Propane layers of each PCU. Furthermore, contrary to the work presented in Kuiper et al. (2004), we now used data from *all* three xenon layers of each PCU, namely, employing data from the (deeper) middle and lower xenon layers considerably improves the signal-to-noise ratio for energies above ~ 10 keV. This allows us to better characterize the hard (> 10 keV) X-ray properties of AXPs.

The number of active PCUs at any time was changing, therefore, we treated the five PCUs constituting the PCA separately. Good time intervals have been determined for each PCU by including only time periods when the PCU in question is on, and during which the pointing direction is within 0.05° from the target, the elevation angle above Earth's horizon is greater than 5° , a time delay of 30 minutes since the peak of a South-Atlantic-Anomaly passage holds, and a low background level due to contaminating electrons is observed. These good time intervals have subsequently been applied in the screening process to the data streams from each of the PCUs (e.g. see Table 1 for the resulting screened exposure of PCU-2 per observation run).

Next, for each sub-observation the arrival times of the selected events (for each PCU unit) have been converted to arrival times at the solar system barycenter (in TDB (=barycentric dynamical time) time scale; DE200 solar system ephemeris) using the instantaneous spacecraft position and the celestial positions of the selected sample of AXPs. In this work we used for the AXP positions those obtained by the Chandra X-ray observatory with a typical position accuracy of about $0''.5$ (for 1RXS J1708-4009, see Israel et al. (2003); for 4U 0142+61, see Patel et al. (2003); for 1E 2259+586, see Patel et al. (2001); for 1E 1048.1-5937, see Wang & Chakrabarty (2002); Israel et al. (2002); and finally for 1E 1841-045, see Wachter et al. (2004)).

These barycentered arrival times have been folded with available phase connected timing solutions (see for details the relevant section on the timing characteristics for each AXP) using only the first three frequency coefficients (frequency, first and second frequency time derivatives at a certain epoch) to obtain pulse phase distributions for selected energy windows. Combining now the phase distributions from the various PCUs for energies between ~ 2 and 10 keV we obtained for each sub-observation pulse profiles, which deviate from uniformity at significances well above 5σ for each of the AXPs in our sample. For the calculation of these significances we applied in this work the *bin-free* Z_n^2 statistic (Buccheri et al. 1983), which behaves as a χ^2 distribution for $2n$ degrees of freedom (n =number of harmonics). However, phase shifts between the sub-observations made a direct combination of the pulse profiles to obtain (very) high-statistics *time-averaged* pulse profiles impossible. Therefore we correlated the pulse phase distribution of each sub-observation with a chosen initial template and

applied the measured phase shifts to obtain an aligned combination with much higher statistics. The correlation is then once repeated with, instead of the initially chosen template, the aligned combination from the first correlation to obtain the final summed profile (see e.g. de Plaa et al. 2003, for a similar iterative method applied for PSR B0540-69).

The net result is a set of aligned high-statistics pulse profiles in 256 energy channels for each of the AXPs in our sample. It should be noted that these profiles are *time-averaged* profiles ignoring possible temporal variations in shape and/or pulsed fraction (see e.g. Rea et al. (2005) for 1RXS J1708-4009; Rea et al. (2006) for 4U 0142+61; and Gavril & Kaspi (2004); Tiengo et al. (2005) for 1E 1048.1-5937).

HEXTE operated in its default rocking mode during the observations listed in Table 1, allowing the collection of real-time background data from two independent positions $\pm 1.5^\circ$ to either side of the on-source position. For the timing analysis we selected only the on-source data. Good time intervals have been determined using similar screening filters as used in the case of the PCA. The selected on-source HEXTE event times have subsequently been barycentered and folded according to the available ephemerides (see PCA part at the beginning of this section) using again only the first three frequency coefficients. Applying, for each AXP in our sample, the phase shifts as derived from the contemporaneous PCA measurements to the HEXTE phase distributions of each sub-observation we obtained the time averaged HEXTE pulse phase distributions in 256 spectral channels (15 - 250 keV) for the combination of observations listed in Table 1.

3.2. RXTE PCA/HEXTE spectral analysis

Because of the non-imaging nature of the two main RXTE instruments the (total) source-flux estimation relies on accurate time-dependent instrumental and celestial background measurements. Although such models exist for the PCA, the complexity of the near environment of the AXPs in our sample makes it very difficult to derive reliable unbiased total flux estimates with the PCA in the 2-30 keV range. Specifically, all AXPs are located in a narrow strip along the Galactic plane where (large) gradients in the Galactic ridge emission exist (Valinia et al. 1998); 1E 1841-045 and 1E 2259+586 are located in supernova remnants; time-variable strong sources are present near to 4U 0142+61 (Be X-ray binary RX J0146.9+6121), 1E 1048.1-5937 (the enigmatic η Carina) and 1RXS J1708-4009 (e.g. the strong and highly variable X-ray binaries OAO 1657-415 and 4U 1700-377).

The rocking strategy applied during HEXTE operations in principle provides instantaneous background measurements, but also in this case the gradient in the Galactic ridge emission and the possible presence of other (strong) sources in both the on and off-source pointings (very serious for e.g. 1RXS J1708-4009 and 4U 0142+61) can result in unreliable (background subtracted) total-source-flux measurements. Therefore we abandoned, in contrast to the work presented in Kuiper et al. (2004) for 1E 1841-045 in Kes 73, the derivation of the total-source flux with the non-imaging PCA and HEXTE instruments.

In this work we concentrate on the derivation of the *time-averaged pulsed* PCA/HEXTE spectra of the AXPs in our sample. This can be done by determining the number of pulsed counts in differential PCA/HEXTE energy bands by fitting a

truncated Fourier series

$$N(\phi) = a_0 + \sum_{k=1}^N a_k \cos(2\pi k\phi) + b_k \sin(2\pi k\phi) \quad (1)$$

with ϕ the pulse phase, to the measured pulse phase distributions $N(\phi)$. It turned out that 3 to 5 harmonics ($N = 3/5$) were sufficient to describe the measured distributions accurately for all energy intervals and AXPs in our sample. In the case of the PCA we derived for each PCU the energy response matrix (energy redistribution including the sensitive area) for the combination of observations listed in Table 1 and subsequently took the different PCU (screened) exposure times into account in the construction of the weighted PCU-combined energy response. The pulsed (excess) counts per energy band are fitted in a procedure assuming either an absorbed power-law ($F_\gamma = K \cdot e^{-N_H \cdot \sigma} \cdot E_\gamma^{-\Gamma}$), or an absorbed double power-law ($F_\gamma = e^{-N_H \cdot \sigma} \cdot (K_1 \cdot E_\gamma^{-\Gamma_1} + K_2 \cdot E_\gamma^{-\Gamma_2})$) or an absorbed black body plus power-law ($F_\gamma = e^{-N_H \cdot \sigma} \cdot (K \cdot E_\gamma^{-\Gamma} + K_{bb} \cdot E_\gamma^2 / (\exp(E_\gamma/kT) - 1))$) photon spectrum folded through the PCU-combined energy response.

In the spectral “deconvolution” process of the HEXTE total pulsed counts in almost all cases⁴ the on-axis cluster A and B energy response matrices have been employed taking into account the (slightly) different screened on-source exposure times for each cluster. The exposure times have been corrected for the considerable deadtime effects.

3.3. INTEGRAL timing analysis

The first step in an INTEGRAL timing analysis is to obtain a set of science windows for which the angular distance between instrument pointing direction and target is within 14.5° to ensure that (a part of) the detector plane is illuminated by the target. The resulting list is further screened on erratic (ISGRI) count rate variations, indicative for particle effects due to Earth radiation belt passages or solar flare activities. These science windows are excluded for further analysis. Next, only events with rise times between 7 and 90 (see Lebrun et al. 2003, for definition), detected in *non-noisy* ISGRI detector pixels which have an illumination factor of more than 25% (i.e. at least 25% of a detector pixel must have been illuminated by the target) are passed for further analysis. The on-board event time stamps are corrected for known instrumental (fixed), ground station and general time delays in the on-board time vs. TT (Terrestrial Time) correlation (see e.g. Walter et al. 2003). The resulting event times in TT of the selected events are barycentered (using the JPL DE200 solar system ephemeris) adopting the Chandra X-ray positions of the AXPs and the instantaneous INTEGRAL orbit information. These barycentered events are finally folded using an appropriate timing model ($\nu, \dot{\nu}, \ddot{\nu}$ and the epoch) to yield pulse phase distributions for different energy bands between 20 and 300 keV. The timing models (phase connecting ephemerides) are based on publicly available RXTE monitoring data of AXPs. Ephemerides have been generated for two AXPs in our sample, 1RXS J1708-4009 and 1E 1841-045, because at the INTEGRAL epoch (MJD > 52668 and MJD > 52698 for 1RXS J1708-4009 and 1E 1841-045, respectively) these were not available from existing literature (see Table 3; all with very small RMS values, required for extracting the weak pulsed signals).

⁴ For HEXTE pointings with the target (AXP) far off-axis e.g. 4U 0142+61 during an observation of HMXB RX J0146.9+6121, we took the reduction in the effective sensitive area due to the collimator response into account

TABLE 3

PHASE COHERENT EPHEMERIDES FOR 1RXS J1708 - 4009 AND 1E 1841-045, DERIVED FROM RXTE PCA MONITORING DATA AND VALID FOR THE ANALYZED INTEGRAL OBSERVATIONS.

AXP	Start [MJD]	End [MJD]	Epoch [MJD,TDB]	ν [Hz]	$\dot{\nu}$ $\times 10^{-13}$ Hz/s	$\ddot{\nu}$ $\times 10^{-22}$ Hz/s ²	RMS
1RXS J1708 - 4009	52590	52939	52590.0	0.09089812328(36)	-1.59836(30)	0.00(Fixed)	0.012
1E 1841-045	52726	52982	52726.0	0.0848972590(50)	-3.2217(85)	4.22(83)	0.015

3.4. INTEGRAL spectral analysis

The INTEGRAL IBIS ISGRI spectral analysis applied in our study is based on OSA 4.1 programs producing sky mosaics for the combination of many science windows in different energy bands (Goldwurm et al. 2003). The resulting dead-time corrected ISGRI source-count rates per energy band are referenced to count rates measured from the Crab in similar energy bands (Crab calibration observations during INTEGRAL Revs. 102/103 were used).

We used for the total Crab photon emission spectrum the following spectrum derived by Willingale et al. (2001) based on XMM-Newton observations of the Crab at energies between 0.3 and 10 keV: photon index $\Gamma = 2.108(6)$ with a normalization at 1 keV of 9.59(5) ph/(cm²s keV).

We verified the validity of the extrapolation of this spectrum to energies between 15 and 250 keV using RXTE HEXTE Crab data. The HEXTE data utilized is from a long dedicated RXTE Crab observation (obs. id. 40805), performed between 17-31 March 1999 and 18-19 Dec. 1999, yielding dead time corrected cluster 0 and 1 exposures of 22.7 and 23.8 ks, respectively. Applying an overall (energy independent) normalization factor of 1.087 to be consistent with the BeppoSAX LECS/MECS/PDS spectrum (Kuiper et al. 2001) the derived 15-250 keV HEXTE Crab total spectrum connects smoothly to the 0.3-10 keV Crab total spectrum derived by Willingale et al. (2001). The HEXTE Crab total spectrum can best be described by a power-law model with an energy dependent photon index as given below:

$$F_{\gamma} = 1.5703(14) \times (E_{\gamma}/0.06355)^{-2.097(2)-0.0082(16) \cdot \ln(E_{\gamma}/0.06355)} \quad (2)$$

In Eq.2, F_{γ} is expressed in ph/(cm²s MeV) and E_{γ} in MeV. Up to $\sim 180-200$ keV the extrapolation of the spectrum given by Willingale et al. (2001) overlaps the HEXTE spectrum, and thus provides a proper representation for the ISGRI energy range we are effectively dealing with.

Therefore, our method for deriving ISGRI spectra enables us to determine the 20-300 keV AXP spectra without detailed knowledge of the instrument energy response, which at the time of our analysis still contained significant uncertainties. Thus, we derive from these spatial analyses total source spectra (sum of pulsed and unpulsed components).

For the construction of spectra for the pulsed components we extracted count rates from the phase distributions similarly as was done for the RXTE light curves. For the conversion to pulsed fluxes, also in this case, the Crab pulsed signal in the HEXTE 15 - 250 keV range (obs. id. 40805) was used as a reference source. This pulsed HEXTE spectrum is properly described by:

$$F_{\gamma} = 0.4693(21) \times (E_{\gamma}/0.04844)^{-1.955(7)-0.0710(78) \cdot \ln(E_{\gamma}/0.04844)} \quad (3)$$

over the entire 15-250 keV energy range. This model has been verified on the pulsed ISGRI spectrum of PSR B1509-58 data, yielding consistent results as reported in Kuiper et al. (1999).

3.5. COMPTEL spatial analysis

During the long mission lifetime of CGRO (April, 1991 – May, 2000), most of the sky, particularly the Galactic Plane, has been viewed with long exposures. We used the exposure accumulated for each source over the total mission duration, amounting for 1RXS J1708 - 4009 5.3 Ms, 4U 0142+61 4.2 Ms, 1E 2259+586 4.9 Ms, 1E 1048.1 - 5937 4.8 Ms, and for 1E 1841-045 4.2 Ms. Skymaps and source parameters can be derived with the maximum likelihood method, which is implemented in the standard COMPTEL data analysis package. See for the implementation of the maximum likelihood method for data from a Compton telescope (de Boer et al. 1992), and for the specific treatment of the instrumental background structure in the COMPTEL data space (Bloemen et al. 1994). For the analysis and data selections we followed the approach described by Zhang et al. (2004). Standard energy intervals were selected for the analysis: 0.75 – 3 MeV, 3 – 10 MeV and 10 – 30 MeV. For each of these energy intervals and for each AXP the source flux (or upper limit) was measured at the known source position in the maximum likelihood skymaps.

4. 1RXS J1708 - 4009

1RXS J1708 - 4009 was discovered in 1996 during the ROSAT (0.1-2.4 keV) all sky survey. X-ray pulsations at a 11-s period were subsequently detected with ASCA (Sugizaki et al. 1997). Its 0.8-10 keV spectrum turned out to be very soft and its general X-ray properties pointed to an AXP membership (see e.g. Israel et al. 1999a; Kaspi et al. 1999). From regular RXTE PCA monitoring observations performed between Jan. 1998 and June 1999 a phase-coherent timing solution was obtained by Kaspi et al. (1999). This demonstrated a high level of rotation stability. Since these early monitoring observations, however, the source experienced two glitches - one in Sept./Oct. 1999 and a second in April 2001 - each with different recovery behaviour (Kaspi et al. 2000; Kaspi & Gavril 2003; Dall'Osso et al. 2003). For the period between the two glitches Gavril & Kaspi (2002) presented a phase-coherent timing solution with a positive $\ddot{\nu}$ indicative for a long-term glitch recovery.

The morphology of the X-ray pulse profile of 1RXS J1708 - 4009 is changing as a function of energy (e.g. Sugizaki et al. 1997; Israel et al. 2001; Gavril & Kaspi 2002). Phase-resolved spectral analyses indeed showed significant spectral variations with pulse-phase, most pronounced in the photon power-law index (e.g. Israel et al. 2001; Rea et al. 2003, 2005). Furthermore, the total phase-averaged unabsorbed 0.5-10 keV X-ray flux and photon spectral index appear to be time variable in a correlated way, with maximal fluxes and hardest spectra near

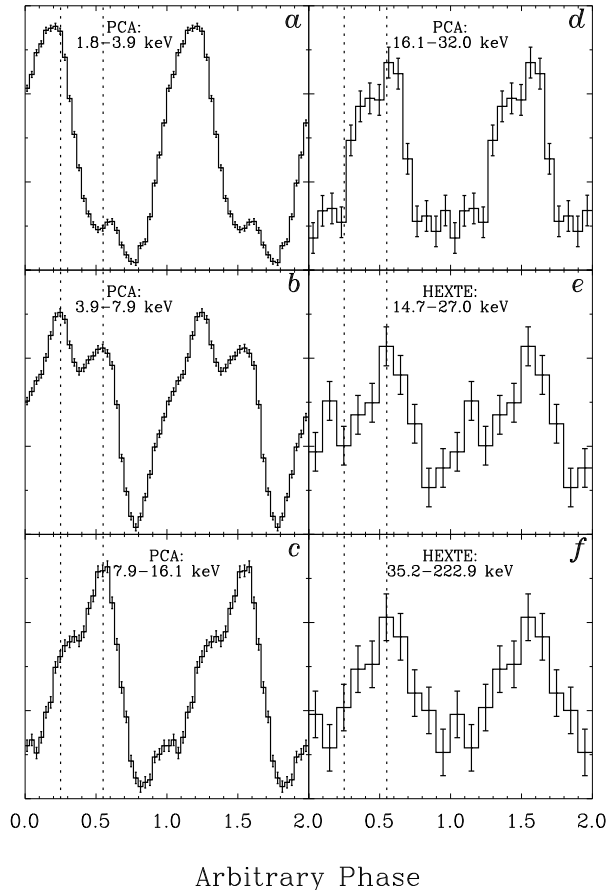


FIG. 1.— RXTE PCA/HEXTE pulse profiles of 1RXS J1708-4009 for energies in the range 1.8-222.9 keV combining data collected between 12 Jan 1998 and 26 Oct 2003 (see Table 1). Two cycles are shown for clarity. The vertical dotted lines at phases 0.25 and 0.55 serve as a guide to the eye for alignment comparisons. Note the drastic morphology changes with energy.

the two glitch epochs (Rea et al. 2005).

At optical/IR wavelengths 2 potential counterparts were identified within the Chandra 0'7 HRC-I error circle (see e.g. Israel et al. 2003; Safi-Harb & West 2005, for more details). A search for radio emission at 1.4 GHz from 1RXS J1708-4009 only yielded a 5σ upper limit of 3 mJy at the position of the AXP (Gaensler et al. 2001).

Given the softness of the 0.5-10 keV X-ray spectra, the INTEGRAL detection reported by Revnivtsev et al. (2004) of a point source at the position of 1RXS J1708-4009 between 18 and 60 keV was a big surprise. Below we will present in detail the new high-energy characteristics of this AXP derived in this work: a) the discovery of the pulsed emission above ~ 10 keV (profiles, spectra) using RXTE PCA/HEXTE and IBIS ISGRI data; b) ISGRI and COMPTEL results on the total emission.

4.1. 1RXS J1708-4009 timing characteristics

4.1.1. RXTE PCA/HEXTE pulse profiles

Applying the timing analysis procedures outlined in Sect. 3.1 to the full set of RXTE observations of 1RXS J1708-4009 listed in Table 1, resulted in a compilation of high-statistics *time-averaged* PCA/HEXTE pulse profiles for energies between ~ 2 –220 keV (see Fig. 1). The ephemerides used in the folding/correlation process (see Sect. 3.1) are given in Kaspi et al. (2000); Gavril & Kaspi (2002); Kaspi & Gavril (2003). For

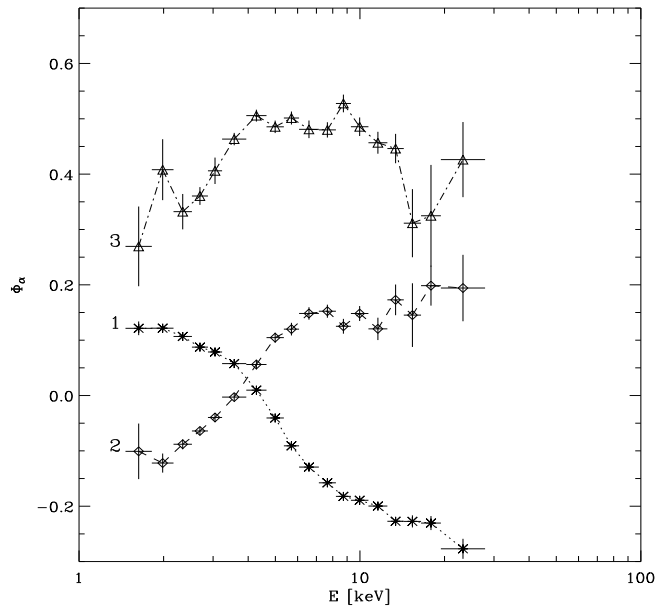


FIG. 2.— Phase angles as a function of energy for the first 3 harmonics used in the truncated Fourier series fit (see Eq. 1) of the RXTE PCA pulse profiles of 1RXS J1708-4009. The harmonics are labeled with their corresponding number.

the first time pulsed emission is detected above ~ 10 keV: the non-uniformity significance of the 16.1-32.0 keV PCA pulse phase distribution (see Fig.1d) is 14.2σ applying a Z_2^2 -test and the HEXTE 35.2-222.9 keV profile (see Fig.1f) deviates from uniformity at a 5.2σ level. Above 35.2 keV the significances in the HEXTE 35.2-64.1 and 74.3- 222.9 keV bands (the intermediate energy window with a large instrumental background feature has been omitted) are both 3.75σ . Drastic morphology changes with energy are visible. The decomposition of the pulse profiles in terms of a finite number of harmonics (see Eq. 1) provides a means to visualize a change in morphology with energy. The power ($a_k^2 + b_k^2$, see Eq.1), derived from the time-averaged PCA pulse profiles of 1RXS J1708-4009, in the first harmonic is dominant over the power in the second and third harmonics, and the power in harmonics with $k \geq 4$ can be neglected (see also Gavril & Kaspi 2002). From Eq. 1 one can define a phase angle $\Phi_\alpha^k = \arctan(a_k/b_k)$ for each harmonic k . The energy dependence of Φ_α^k for the first three harmonics is shown in Fig. 2. For each harmonic it reveals a very smooth variation of the phase angle with energy. The shape of the profile is changing drastically between 2 and 10 keV. For energies above ~ 15 keV the phase angles for the 3 considered harmonics seem to converge to constant values, a necessary condition for stable pulse shapes.

4.1.2. INTEGRAL IBIS ISGRI pulse profiles

We also performed a timing analysis for 1RXS J1708-4009 using IBIS ISGRI data. Data from science windows taken during INTEGRAL Revs. 36-120 satisfying our $14^\circ 5'$ off-axis constraint were included (effective on-axis exposure after screening $\sim 1,360$ ks). The processing followed the guidelines presented in Sect. 3.3 using the 1RXS J1708-4009 ephemeris generated from RXTE monitoring observations, given in Table 3. In the integral 20-300 keV ISGRI band we obtained a non-uniformity significance of 5.9σ applying a Z_2^2 test, which is comparable to the HEXTE result. In differential energy bands we found: 20-75 keV, 4.3σ , and 75-300 keV 3.6σ (see Fig. 3

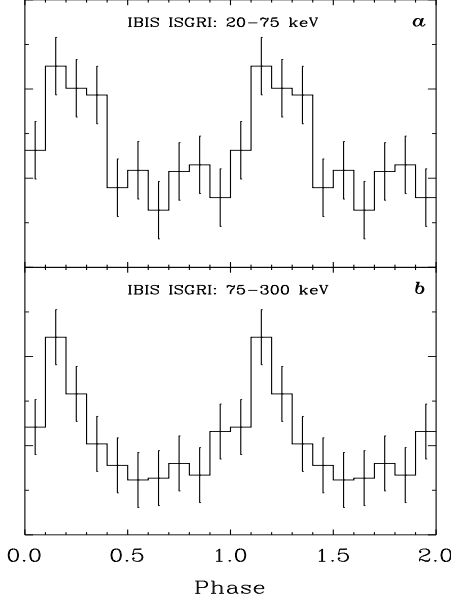


FIG. 3.— INTEGRAL IBIS ISGRI pulse profiles of 1RXS J1708-4009 for two energy ranges. The non-uniformity significances are 4.3σ and 3.6σ for 20-75 keV and 75-300 keV, respectively. Pulse maxima are found near phase ~ 0.2 , corresponding to phase 0.55 in Fig. 1.

for the corresponding pulse profiles). The HEXTE and the ISGRI profiles above 75 keV are very similar, and suggest that the hard-X-ray 1RXS J1708-4009 profile exhibits less structure than found below 10 keV. From these initial ISGRI timing results it is clear that highly significant profiles can be expected in the near future when significantly more IBIS ISGRI data on this source become available.

4.2. 1RXS J1708-4009 spectral characteristics

In this section we present new high-energy spectral information above 2.5 keV up to 30 MeV for 1RXS J1708-4009: (a) (time-averaged) pulsed emission from RXTE PCA and HEXTE; (b) pulsed emission from INTEGRAL IBIS ISGRI; (c) total (pulsed and unpulsed) emission from ISGRI and upper limits to the total emission from CGRO COMPTEL. Finally, the new spectra are compared with spectra reported earlier for energies below 10 keV (Rea et al. 2003, 2005, for BeppoSAX LECS/MECS 0.4-10.8 keV and XMM Newton MOS/PN 0.5-10 keV, respectively).

4.2.1. RXTE PCA/HEXTE pulsed spectrum

The spectral procedures employed for the RXTE PCA and HEXTE data (see Sect. 3.2) resulted in a high-statistics determination of the spectrum of the time-averaged pulsed emission of 1RXS J1708-4009 in the ~ 2.5 –220 keV energy range. The PCA (aqua) flux values are derived assuming an absorbed double power-law spectral model, and are shown in a νF_ν representation in Fig. 4. Also drawn is the best fitting spectral model to the PCA data points (2.5-36.9 keV; $\chi_r^2 = 1.11$ for 12 degrees of freedom; dashed line). The assumed absorbing Hydrogen column density N_H in the spectral fit was $1.36 \times 10^{22} \text{ cm}^{-2}$ (Rea et al. 2003). The two power-law components become equally strong at $E_{\text{cross}} = 21.7 \pm 2.4$ keV: below this energy the power-law component with index $\Gamma_1 = 2.60 \pm 0.01$ dominates and above a component with very hard spectrum, index $\Gamma_2 = -0.12 \pm 0.07$. It is clear that the pulsed spectrum hardens

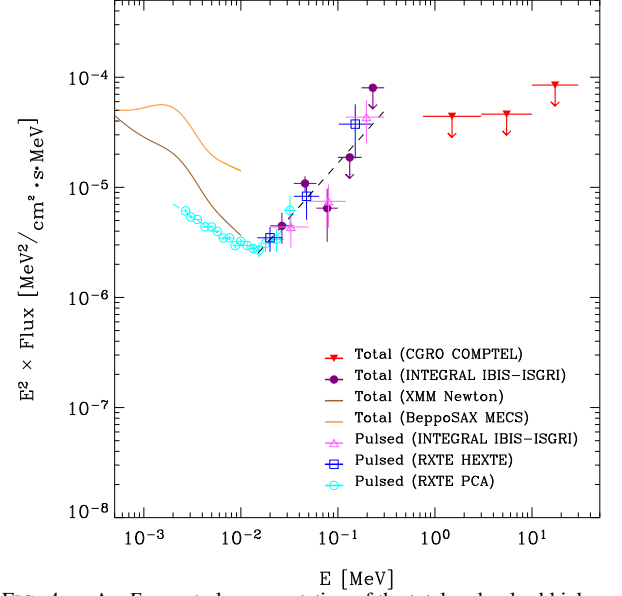


FIG. 4.— A νF_ν spectral representation of the total and pulsed high-energy emission from 1RXS J1708-4009. The aqua (PCA), blue (HEXTE) and magenta (IBIS ISGRI) data points show the *time-averaged* 2.5-300 keV pulsed spectrum. The black dashed line shows the best power-law model fit to the combination of PCA, HEXTE and ISGRI pulsed flux values for energies above ~ 15 keV. The other measurements refer to the total emission spectrum: 0.5-10 keV, BeppoSAX LECS/MECS and XMM Newton spectral models at different epochs (Rea et al. 2003, 2005); 20-300 keV time-averaged (Revs. 36-106) IBIS ISGRI spectrum; and 0.75-30 MeV, time-averaged CGRO COMPTEL 2σ upper-limits. Note the drastic hardening of the pulsed spectrum near 20 keV. The COMPTEL upper limits require another spectral break somewhere between 300 and 750 keV.

dramatically above 20 keV, however, the spectrum has to soften considerably to be consistent with the index of 1.01(12) derived from a combination of PCA, HEXTE and IBIS ISGRI pulsed flux measurements for energies $\gtrsim 15$ keV (see Sect. 4.2.2). The HEXTE flux values (simultaneously derived) are fully consistent with the upturn found in the PCA spectrum (see Fig. 4, blue datapoints).

4.2.2. INTEGRAL IBIS ISGRI pulsed spectrum

Pulse profiles for 1RXS J1708-4009 have been generated in three energy intervals from 20 to 300 keV using IBIS ISGRI data from Revs 36-120. The pulsed (excess) count rates were determined and transformed to pulsed flux values, calibrated on the pulsed Crab spectrum. The three flux values are also included in Fig. 4. They are consistent with the data points derived from RXTE HEXTE for the same energy window, but measured at different epochs. Within the present statistical accuracies there is no indication for long-term flux variability above 20 keV, contrary to the reported strong flux variability for energies below 10 keV, clearly visible in Fig. 4. A power-law fit through the PCA, HEXTE and IBIS ISGRI pulsed flux measurements for energies above 15 keV yielded a photon index of 1.01 ± 0.12 . This model is shown in Fig. 4 as a dashed black line for the 15-300 keV energy range. There is no indication yet for a second spectral break up to 300 keV.

4.2.3. INTEGRAL IBIS ISGRI and COMPTEL total spectrum

1RXS J1708-4009 was detected at a 6.5σ level in the 18-60 keV energy band by Revnivtsev et al. (2004) using IBIS ISGRI data from a 2 Ms ultra deep INTEGRAL survey of the Galactic center region performed in Aug. - Sept. 2003 (INTEGRAL

Revs. 104-107 & 111-113). Its 18-60 keV flux was 2.2 ± 0.3 mCrab. In this work we analyzed (almost independent) IBIS ISGRI data from all publicly available INTEGRAL observations performed between revolutions 36 and 106 in which the angular distance between 1RXS J1708-4009 and the science window pointing was $\leq 14.5^\circ$. The effective on-axis exposure after screening is about 974 ks. Mosaic images have been made using OSA 4.1 procedures for 5 broad differential energy bands, 20-35, 35-60, 60-100, 100-175 and 175-300 keV, in order to determine the total hard X-ray/soft γ -ray spectrum of this AXP. 1RXS J1708-4009 was detected significantly only in the 20-35 and 35-60 keV energy bands with flux levels consistent with the 18-60 keV flux measurement by Revnivtsev et al. (2004). The resulting IBIS ISGRI spectral measurements are shown as purple data points in Fig. 4. Unfortunately, the statistics in these IBIS ISGRI data points are still too poor to constrain the underlying emission model in the 20-300 keV range: the fit quality specified by a reduced χ_r^2 of 1.77 for 3 d.o.f. assuming a simple power-law model is still acceptable; the resulting photon index is 1.44 ± 0.45 , slightly softer than, but consistent with, the pulsed flux spectrum derived from the combined fit to the PCA, HEXTE and IBIS ISGRI pulsed flux measurements at ≥ 15 keV.

Finally, at energies above 750 keV till 30 MeV we generated skymaps using all CGRO COMPTEL observations with 1RXS J1708-4009 in its field of view, spread over its full 9 year mission lifetime. The source was not seen for any of the standard energy intervals, and we derived (2σ) flux upper limits, also shown in Fig. 4.

4.2.4. Discussion of spectra and pulsed fraction of 1RXS J1708-4009

Comparing the total IBIS ISGRI spectrum derived in the spatial analysis with the pulsed time-averaged spectra from RXTE PCA/HEXTE and ISGRI, we see that the 1RXS J1708-4009 emission is consistent with about 100% pulsation for energies in excess of 20 keV. For energies below 20 keV, the situation is very different. To highlight this, we included in Fig. 4 the emission models (best spectral fits) for the total 0.5-10 keV X-ray spectra measured at two different epochs (Rea et al. 2003, 2005, for BeppoSAX LECS/MECS 0.4-10.8 keV and XMM Newton MOS/PN 0.5-10 keV, respectively). Given the apparent drastic spectral change in both shape and normalization for energies below 10 keV we cannot uniquely quantify the pulsed fraction as a function of energy comparing with the time-averaged high-statistics PCA pulsed flux measurements. Obviously, the BeppoSAX measurement during August 2001 does not connect to the RXTE/INTEGRAL spectra. 1RXS J1708-4009 was apparently in a (very) different high state during the BeppoSAX observation, which took place in the recovering phase from the secondly reported glitch (see Rea et al. 2005). The XMM Newton spectrum connects very smoothly to the total spectrum measured by INTEGRAL, and suggests a variation in pulsed fraction from $\sim 25\%$ at 2 keV to 100% at 20 keV. Our time averaged results for the total and pulsed emission above 20 keV suggest a very stable behaviour of this AXP at these higher energies. It seems that a stable and very hard pulsed component is dominating the emission at these energies. Interestingly, the COMPTEL MeV upper limits then require a spectral break in this hard spectrum of 1RXS J1708-4009 somewhere between 300 and 750 keV.

5. 4U 0142+61

4U 0142+61 was discovered in the early seventies by the scanning *Uhuru* X-ray observatory (see e.g. Forman et al. 1978). The X-ray sky survey performed by the SSI (1.5-20 keV) on *Ariel V* (Warwick et al. 1981) and X-ray observations by SAS-3 and HEAO-1 confirmed the source and refined its position considerably (see e.g. Reid et al. 1980, for an X-ray position with $23''$ accuracy). Data from the non-imaging ME collimator ($45'$ FWHM) aboard EXOSAT revealed a coherent 25 minute signal, which was later absent in two shorter EXOSAT observations (White et al. 1987). These authors also presented more accurate ($3''/2$) positional information for 4U 0142+61 using both EXOSAT LEIT and *Einstein* (HEAO-2) HRI data and demonstrated the lack of a bright optical counterpart, ruling out the presence of a massive companion.

The discovery in ROSAT all-sky survey data of a Be/X-ray binary, RX J0146.9+6121, by Motch et al. (1991) at only $24'$ from 4U 0142+61 showed that there had been source confusion. Revisiting the EXOSAT 1985 data, Israel et al. (1994) discovered a 8.7 s periodicity, only detectable in the 1-3 keV energy band. Finally, using ROSAT PSPC data, Hellier (1994) unambiguously demonstrated that the 8.7 s periodicity originated from 4U 0142+61 and the 25 min signal from the Be/X-ray binary RX J0146.9+6121, which moreover showed transient activity.

A good quality phase-averaged 0.5-10 keV X-ray spectrum of 4U 0142+61 was derived by White et al. (1996) analyzing ASCA SIS/GIS data. The physically most plausible model consists of an absorbed black-body plus power-law component with best-fit model parameters: black-body temperature $0.386(5)$ keV; photon-index $3.67(9)$ and N_H $9.5(4) \times 10^{21} \text{ cm}^{-2}$. These authors, using data covering a much wider time baseline, also confirmed the spin-down timescale of $\sim 1.2 \times 10^5$ year, reported earlier by Hellier (1994). The spin-down energy release is much lower than the observed X-ray luminosity, thereby excluding 4U 0142+61 to be a spin-down powered pulsar.

RXTE monitoring observations since November 1996 (Gavril & Kaspi 2002) proved that 4U 0142+61 is a very stable rotator, like spin-down powered pulsars, and ASCA data taken in a 2 year gap of RXTE observations seemed to indicate a pulsar-like glitch in its rotation behaviour (Mori et al. 2005). Time-averaged RXTE PCA pulse profiles in two different energy bands showed significant morphology changes with energy, consistent with earlier results of much lower significance (Israel et al. 1994; White et al. 1996; Israel et al. 1999b).

Recent X-ray observations of 4U 0142+61 by Chandra (Juett et al. 2002; Patel et al. 2003) and XMM (Göhler et al. 2005) improved not only the positional accuracy down to $0''.5$, but also provided high-quality (phase-resolved) spectra which are mutually consistent and appeared featureless. The phase-resolved spectra showed significant changes in photon-index and black body temperature as a function of pulse phase.

At lower energies, Hulleman et al. (2000) discovered a faint optical counterpart within the 4U 0142+61 *Einstein* X-ray error circle, followed by the detection of optical pulsations with a high pulsed fraction from this counterpart (Kern & Martin 2002). No radio counterpart has been found yet (Gaensler et al. 2001).

At higher energies the discovery was reported by den Hartog et al. (2004) of hard X-rays/soft γ -rays (20 – 150 keV) in INTEGRAL IBIS ISGRI data of a deep 1.6 Ms observation of the Cassiopeia region. A detailed analysis of this long obser-

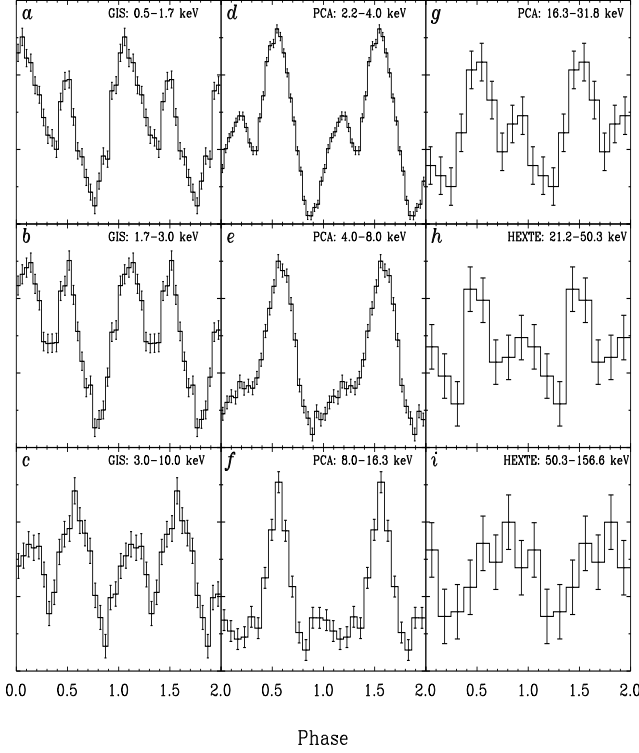


FIG. 5.— ASCA GIS, RXTE PCA and HEXTE pulse profiles of 4U 0142+61 for energies in the range 0.5–156.6 keV. Two cycles are shown for clarity. The RXTE profiles shown in panels d–i are time-averaged and based on observations performed between March 1996 and September 2003. The GIS profiles (panels a–c) are from ASCA observations performed in July/August 1999 totaling ~ 120 ks of exposure. For the first time significant deviations from uniformity are visible at energies > 8 keV: Z^2_2 is 16.6σ and 5.9σ for the PCA 8.0–16.3 and 16.3–31.8 keV bands, respectively; the significances for the HEXTE profiles are 3.4σ and 2.0σ for the 21.2–50.3 and 50.3–156.6 keV bands. Note the drastic morphology changes with energy.

vation (den Hartog et al. 2006), proved that the spectrum in this energy range is very hard with power-law photon index $\Gamma = 0.73 \pm 0.17$. The X-ray luminosity between 20 and 100 keV was found to be $5.9 \times 10^{34} \text{ erg s}^{-1}$, a factor 440 higher than the rotational energy loss. They also reported flux upper limits from COMPTEL between 0.75 and 30 MeV, which indicated that the hard spectrum has to break/bend between ~ 100 keV and 0.75 MeV.

In this work we will present for 4U 0142+61: a) for the first time the PCA/HEXTE timing and spectral results for energies above ~ 8 keV using all publicly available RXTE data, b) timing and spectral results from analysis of ASCA GIS 0.5–10 keV data, and c) a spectrum with higher statistical accuracy of the total emission as seen by IBIS ISGRI over the 20–300 keV energy range using all available public, Core Program (Galactic plane scans; 4U 0115+63 Target of Opportunity Observation) and Open Time (Cassiopeia region; IGR J00291+5934 TOO) INTEGRAL data.

5.1. 4U 0142+61 timing characteristics

Time-averaged RXTE pulse profiles of 4U 0142+61 are shown in Fig. 5 for energies between 2.2 and 156.6 keV (PCA/HEXTE). We used in the folding/correlation process (see Sect. 3.1) the ephemerides given by Gavril & Kaspi (2002). The 2.2–4.0 keV PCA profile (panel d) shows two distinct pulses near phases 0.2 and 0.55. Moving up in energy the pulse near 0.2 loses significance and is gone for energies above ~ 8 keV (panels e–f).

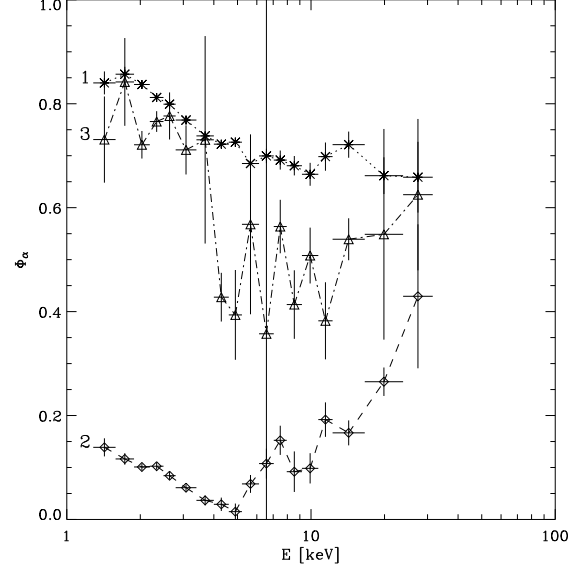


FIG. 6.— Phase angles as a function of energy for the first 3 harmonics of the truncated Fourier series fit of the RXTE PCA pulse profiles of 4U 0142+61. Note the sign reversal of the energy derivative of Φ_α for the second harmonic near 5 keV.

Instead above ~ 8 keV a feature near phase 0.9 pops up, which is visible up to ~ 50 keV (panels f–h). Above 50 keV (panel i) the phase region between the two pulses at 0.55 and 0.9 seems to be filled in by a new component, but the statistics is too poor to make stringent conclusions.

Most importantly, we detect for the first time significant pulsed emission from 4U 0142+61 at energies above ~ 8 keV: 16.6σ and 5.9σ for the PCA 8.0–16.3 and 16.3–31.8 keV bands, respectively. To investigate further the increase in strength of the pulse near phase 0.2 towards lower energies, we extended the energy baseline by including also our results from a timing analysis of ASCA GIS (0.5–10 keV) data from observations performed in July/August 1999 (~ 120 ks exposure). Three profiles (energy bands 0.5–1.7, 1.7–3.0 and 3.0–10 keV) are shown in panels a–c of Fig. 5. Indeed, for the pulse near phase 0.2 the trend of increasing strength towards lower energies is continued in the ASCA GIS 0.5–1.7 and 1.7–3.0 keV energy ranges.

A decomposition of the PCA pulse profiles in terms of 5 Fourier harmonics shows that above 2 keV most of the signal power is embedded in the first harmonic which becomes more and more dominant over the power in the second harmonic, the next powerful harmonic, with increasing energy. Below ~ 2 keV the power in the second harmonic is dominant over that in the first. The behaviour of the phase angles Φ_α^k as a function of energy for the first three harmonics is shown in Fig. 6. Similar to 1RXS J1708–4009 but with different trends, also now a smooth energy dependency of Φ_α^k is shown for each harmonic with significant power. The exception is the derivative of Φ_α^2 to energy which flips sign near 5 keV. For 4U 0142+61 it is less obvious that the pulse profile remains stable above 20 keV, than seems to be the case for 1RXS J1708–4009.

5.2. 4U 0142+61 spectral characteristics

In this section we present: a) the *time-averaged* pulsed spectrum (2.2–102 keV) of 4U 0142+61 based on RXTE PCA and HEXTE measurements. The pulsed spectrum is extended down to 0.8 keV by including our spectral results from the ASCA

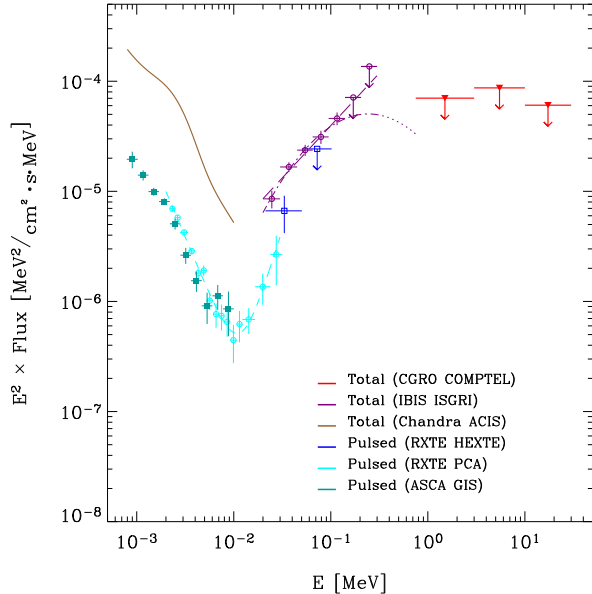


FIG. 7.— A νF_ν spectral representation of the total and pulsed high-energy emission from 4U 0142+61. The aqua, blue and dark cyan data points/curves represent the pulsed emission component of the spectrum (0.8-102 keV) based on RXTE PCA/HEXTE observations (time-averaged) and ASCA GIS. Note the dramatic hardening of the pulsed spectrum near 10 keV. The other measurements refer to the total emission spectrum: 0.8-10 keV, Chandra ACIS (Patel et al. 2003), 20-300 keV, INTEGRAL IBIS ISGRI (this work) and 0.75-30 MeV, CGRO COMPTEL (den Hartog et al. 2006). The COMPTEL 2σ upper limits require a spectral break somewhere between 140 and 750 keV.

GIS observations (~ 120 ks); b) the *time-averaged* total (pulsed and unpulsed) spectrum from our analysis of INTEGRAL IBIS ISGRI skymaps (20-300 keV), in comparison with that from Chandra ACIS-S CC-mode data (0.5-7 keV; Patel et al. 2003) and the CGRO COMPTEL (0.75-30 MeV) upper limits (den Hartog et al. 2006).

5.2.1. RXTE PCA/HEXTE and ASCA GIS pulsed spectrum

Assuming an underlying absorbed ($N_H = 9.3 \times 10^{21} \text{ cm}^{-2}$; Patel et al. 2003) double power-law photon model we fitted the pulsed PCA excess counts (2.2-31.5 keV) in a forward folding procedure (see Sect. 3.2), resulting in a high-statistics time-averaged pulsed spectrum. The best model fit ($\chi_r^2 = 0.7$; d.o.f. 15 - 4) yielded for the soft and hard photon indices $\Gamma_1 = 4.09 \pm 0.04$ and $\Gamma_2 = -0.8^{+0.10}_{-0.07}$, respectively. This is shown as a dashed aqua curve in Fig. 7, together with the “deconvolved” unabsorbed flux values (aqua colored open circles). The power-law model components become equally strong at 11.46 ± 0.64 keV.

The striking spectral hardening of the pulsed emission of 4U 0142+61 around 10 keV is dramatic, much more pronounced than the hardening observed for 1RXS J1708 - 4009.

The HEXTE pulsed flux values (Fig. 7; dark-blue open squares) are in line with the extrapolation of the PCA hard-power-law model component.

The ASCA GIS 0.8-10 keV pulsed flux values which we derived from the July/August 1999 observations are also shown in Fig. 7 (filled squares) and are within the systematic/statistical uncertainties consistent with the time-averaged PCA fluxes in the overlapping energy range. This suggests a rather stable pulsed spectrum both in shape and normalization.

5.2.2. INTEGRAL IBIS ISGRI total spectrum

den Hartog et al. (2006) report the detection and total spectrum of 4U 0142+61 in the 20-100 keV energy range analyzing IBIS ISGRI data from INTEGRAL observations of the Cassiopeia region performed in Dec. 2003 (Revs. 142 - 148). In this work all available INTEGRAL data (open time/core program) have been used from observations made between 3 March 2003 (Rev. 47) and 28 December 2004 (Rev. 269) in which the source was within 14.5° from the pointing axis. The total screened exposure time for the set of accumulated science windows is about 2 Ms, which corresponds to an effective on-axis exposure of about 858 ks. Image mosaics have been generated using OSA 4.1 software in 7 differential energy bands, 20-30, 30-45, 45-65, 65-95, 95-140, 140-205 and 205-300 keV. In these (time-averaged) maps⁵ 4U 0142+61 is clearly detected up to and including the 95-140 keV energy range (7.8 ± 1.0 mCrab). The 20-300 keV flux measurements are shown as purple data points in Fig. 7. A simple power-law fit to these flux points yielded a hard photon index of 1.05 ± 0.11 ($\chi_r^2 = 0.86$ for d.o.f. 6 - 2; the purple dashed line in Fig. 7). The difference with the value (0.73 ± 0.17) reported for the index by den Hartog et al. (2006) is 1.6σ .

5.2.3. Discussion of spectra and pulsed fractions of 4U 0142+61

The INTEGRAL spectrum of the total emission above 20 keV can be compared with the same Chandra spectrum for energies below 10 keV (see Fig. 7 the dark orange solid line; Patel et al. 2003). As is the case for the pulsed spectra above and below ~ 10 keV, these two spectra are drastically different, and together reveal a sharp minimum in luminosity of 4U 0142+61 around 10 keV.

Including now in this high-energy spectral picture the time-averaged CGRO COMPTEL 2σ flux upper limits (red triangles in Fig. 7) from den Hartog et al. (2006) confirms that the power-law model satisfactorily describing the 20-300 keV total spectrum will not extend into the MeV range, but must break somewhere between 140 and 750 keV. To investigate this further, we also fitted a spectral model with an energy-dependent photon index, $F_\gamma = K \cdot E_\gamma^{-(\Gamma + \alpha \ln(E_\gamma))}$, to the 20-300 keV IBIS ISGRI measurements (see Fig. 7 dashed dotted purple line). The model extrapolation towards the MeV energy range is consistent with the COMPTEL upper limits, but the improvement of the fit is insufficient to claim a change in spectral shape in the 20-300 keV window.

Comparing now the total and pulsed high-energy spectra of 4U 0142+61, the Chandra total flux values below 10 keV are about 10 times higher than the time-averaged RXTE PCA and ASCA GIS pulsed flux measurements. This is consistent with pulsed fraction estimates of $\sim 10\%$ reported by Patel et al. (2003) and Göhler et al. (2005) using solely Chandra and XMM Newton data, respectively. The total spectrum measured by INTEGRAL above 20 keV with slope 1.05 ± 0.11 is significantly softer than the pulsed spectrum measured by RXTE above ~ 10 keV with slope $-0.8^{+0.10}_{-0.07}$. As a result, the pulsed fraction appears to vary with energy from $\sim 10\%$ at 20 keV to $\sim 100\%$ between 80 and 100 keV.

6. 1E 2259+586

Near the center of SNR CTB 109 (G 109.1-1.0) a strong compact X-ray source was found by Gregory & Fahlman (1980),

⁵ Be X-ray binary RX J0146.9+6121 at only $24'$ from 4U 0142+61 was detected, fully resolved, only in the first three energy bands.

later dubbed 1E 2259+586, which appeared to be an X-ray pulsar with a period of 3.489(2) s (Fahlman & Gregory 1981). Analyzing more IPC data, this period turned out to coincide with the first harmonic of a fundamental 6.978 s period (Fahlman & Gregory 1983).

No radio enhancement at the position of the X-ray pulsar could be identified down to a level of 0.5 mJy (WSRT, 21 cm; Hughes et al. 1984), 0.2 mJy (VLA, 20 cm; Gregory et al. 1983) and even 50 μ Jy (VLA, 20cm; Coe et al. 1994; Kaspi et al. 2003). On the other hand, the lack of a bright visual counterpart ($V \geq 21$) ruled out a supergiant or massive main-sequence star association (Fahlman & Gregory 1981).

Further X-ray observations of 1E 2259+586 in the eighties with Tenma (Astro-B), EXOSAT and Ginga (Astro-C) (see e.g. Koyama et al. 1987; Morini et al. 1988; Hanson et al. 1988; Koyama et al. 1989; Iwasawa et al. 1992) revealed a steady spin-down, too slow to power the observed X-ray luminosity, and a very soft spectrum. X-ray flux measurements from two different Ginga observations spread ~ 8 months apart indicated considerable flux variations, accompanied with clear pulse morphology changes and probably a decrease in spin-down rate (Iwasawa et al. 1992). The X-ray picture was refined considerably in the nineties using data from BBXRT, ASCA (Astro-D), ROSAT, BeppoSAX and RXTE. Corbet et al. (1995) showed for the first time that a two-component spectral model - black-body plus power-law - could fit the ASCA and BBXRT spectral data satisfactorily without invoking spectral (line) features. This finding was confirmed by Rho & Petre (1997) analyzing ROSAT PSPC, ASCA and BBXRT data simultaneously, and by Parmar et al. (1998) analyzing BeppoSAX LECS and MECS data. RXTE timing measurements (Mereghetti et al. 1998) further tied down earlier limits on the projected semi-axis to 0.03 lts, leaving room only for a white dwarf companion, helium-burning star with mass smaller than $0.8 M_{\odot}$ or a main-sequence star viewed under very small inclination angles.

Kaspi et al. (1999) obtained for the first time a phase coherent timing solution for 1E 2259+586, indicating great stability (rms 0.01 cycles) over the 2.6 year timespan (29-Sept-1996 – 12-May-1999) of their RXTE monitoring observations. This stability makes binary accretion scenarios very unlikely and favours a magnetar interpretation. Additional RXTE monitoring data showed that this rotational stability was maintained throughout an extended 4.5 yr period, although the inclusion of $\dot{\nu}$ was required in the timing model (Gavriil & Kaspi 2002). These authors also found that the pulse morphology did not change significantly with time (cf. Iwasawa et al. 1992, who claimed changes in morphology with time). Moreover, there was no evidence for large variability in the pulsed flux in line with earlier work by Baykal et al. (2000) using RXTE data, but in contrast with the Ginga findings (Iwasawa et al. 1992). Furthermore, Gavriil & Kaspi (2002) showed, convincingly for the first time, that the pulse profile morphology of 1E 2259+586 changes with energy (cf. Hanson et al. 1988, for earlier indications).

Observations with the Chandra X-ray observatory in January 2000 provided an X-ray position with subarcsecond accuracy (Hulleman et al. 2001; Patel et al. 2001). In the $0''.6$ error circle (99%) a very faint ($K_s = 21.7 \pm 0.2$ mag) near-infrared counterpart was identified (Hulleman et al. 2001), excluding models in which the source is powered by disk accretion. The total X-ray (0.5-7.0 keV) spectrum of 1E 2259+586 appeared featureless and could best be described by a combination of a black body

$kT = 0.412(6)$ keV plus power-law $\Gamma = 3.6(1)$ absorbed by a Hydrogen column $N_H = (9.3 \pm 0.3) \times 10^{21} \text{ cm}^{-2}$ (Patel et al. 2001).

In June 2002 RXTE observed an outburst of 1E 2259+586 during which both the pulsed and persistent X-ray emission increased by more than an order of magnitude relative to their quiescent levels (Kaspi et al. 2003). During the course of the observation a spectral softening occurred, and a significant pulse profile change was observed. In the meantime the pulsar underwent a sudden spin-up (glitch) followed by a large increase in spin-down rate lasting for more than 18 days. Furthermore, 80 X-ray bursts were detected during the 14.4 ks RXTE observation with durations ranging from 2 ms to 3 s. The outburst properties of 1E 2259+586 share strong similarities with SGR outburst characteristics unifying thereby conclusively AXPs and SGRs and supporting strongly a magnetar interpretation. More detailed information on the burst characteristics can be found in Gavriil et al. (2004). Woods et al. (2004) presented a comparison of the X-ray emission characteristics of 1E 2259+586 before, during and after the June 2002 outburst using data from XMM-Newton and RXTE. They quantified the changes of the temporal and spectral properties and derived recovery timescales. The X-ray flux increase and subsequent decay can be described by two distinct components: one component linked to the burst activity with a timescale of ~ 2 days and a second component which decays over the course of the year according to a power-law in time ($F \propto t^{\alpha}$) with index $\alpha = -0.22 \pm 0.01$. The latter component behaves similarly in time as the observed near-infrared flux decay (Tam et al. 2004) and thus these seem to be linked to a common physical mechanism likely acting in the pulsar's magnetosphere.

In this work we derived for the first time the time-averaged timing/spectral properties of 1E 2259+586 for energies above ~ 8 keV using archival RXTE PCA/HEXTE data and we compared the pulsed spectrum with the upper limits from IBIS IS-GRI and COMPTEL (den Hartog et al. 2006).

6.1. 1E 2259+586 timing characteristics

The *time-averaged* RXTE PCA/HEXTE pulse profiles combining all observations of 1E 2259+586 listed in Table 1, except the 14.4 ks period of outburst in 2002, are shown in Fig. 8 for energies between 2.2 and 27 keV. In the folding/correlation process (see Sect. 3.1) we used the ephemeris given by Gavriil & Kaspi (2002). The screened PCU-2 exposure amounts ~ 747 ks, while the corresponding dead-time corrected on-source HEXTE exposures are 256.4 and 267.7 ks for cluster-0 and 1, respectively. For the first time significant deviations from uniformity are visible at energies $\gtrsim 8$ keV: Z_2^2 is 10.6σ , 5.2σ and 3.1σ for the PCA 8.3-11.9, 11.9-16.3 and 16.3-24 keV bands, respectively (Fig. 8 panels c-e). The HEXTE sensitivity is still too low to detect the underlying pulsed emission above ~ 15 keV (Fig. 8 panel f).

The morphology of the double-peaked pulse profile changes gradually moving up in energy from 2.2 to 24 keV: the dominant pulse near phase 0.7 in Fig. 8 at energies below ~ 4 keV loses significance with respect to the second pulse near phase 0.25. The latter dominates at energies above ~ 8 keV. Also note the existence of a narrow pulse-like feature in the deepest minimum near phase 0.45, most striking in panel b (4-8.3 keV) of Fig. 8. The latter feature is also clearly visible in Fig. 7c of Gavriil & Kaspi (2002).

More quantitative information on the energy dependency of the pulse morphology can be obtained through a decomposition of the pulse profiles in Fourier components. At least 5 har-

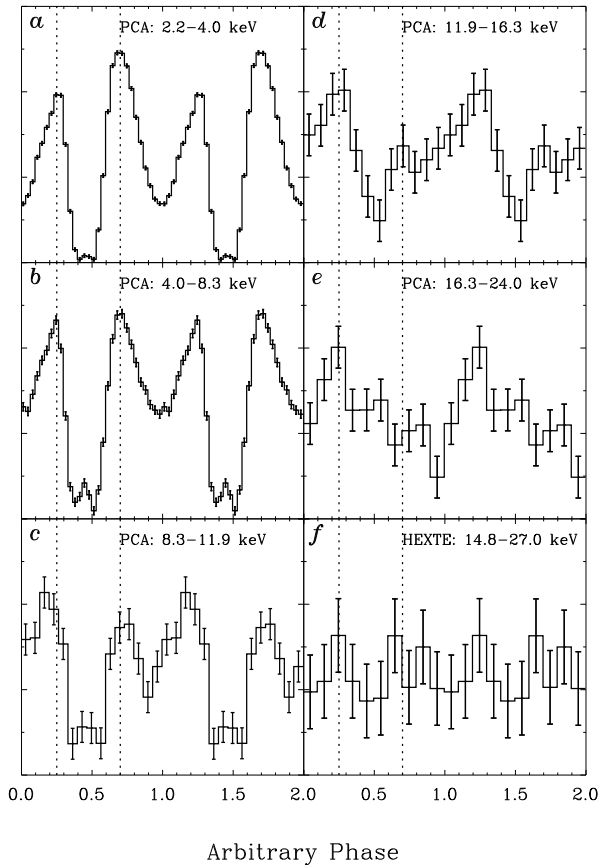


FIG. 8.— RXTE PCA/HEXTE pulse profile collage of 1E 2259+586 for energies in the range 2.2–27.0 keV combining data collected between 29 Sept 1996 and 28 Oct 2003 (see Table 1). Two cycles are shown for clarity. The vertical dotted lines at phases 0.25 and 0.70 serve as a guide to the eye for alignment comparisons. Clear pulse profile morphology changes with energy are present. Pulsed emission is detected up to ~ 24 keV. Note the enhancement within the main valley between the two peaks near phase 0.45, also visible in Fig. 7c of Gavril & Kaspi (2002).

monics are required to adequately fit the profiles in the various energy slices, mainly driven by the existence of the narrow, significant feature in the main valley between the peaks. This was also shown by Gavril & Kaspi (2002). While the power of the second harmonic (2 maxima per cycle) dominates over that of the first up to ~ 10 keV (beyond which they become statistically equally strong) and the phase angle Φ_α^2 of the second harmonic remains more or less at the same position in phase, the first harmonic (broad component) shifts gradually to the right in phase with increasing energy (see Fig. 9). This energy dependent shift reflects the collapse at higher energies of the dominant pulse at low energies near phase 0.7.

6.2. 1E 2259+586 spectral characteristics

In this section the *time-averaged* pulsed spectrum of 1E 2259+586 is derived based on the RXTE PCA & HEXTE observations given in Table 1. The high-energy picture has been completed by comparing our results with the total emission spectrum (2–10 keV) as determined by Patel et al. (2001) and with IBIS ISGRI (20–300 keV) and COMPTEL (0.75–30 MeV) upper limits (den Hartog et al. 2006).

6.2.1. RXTE PCA/HEXTE pulsed spectrum

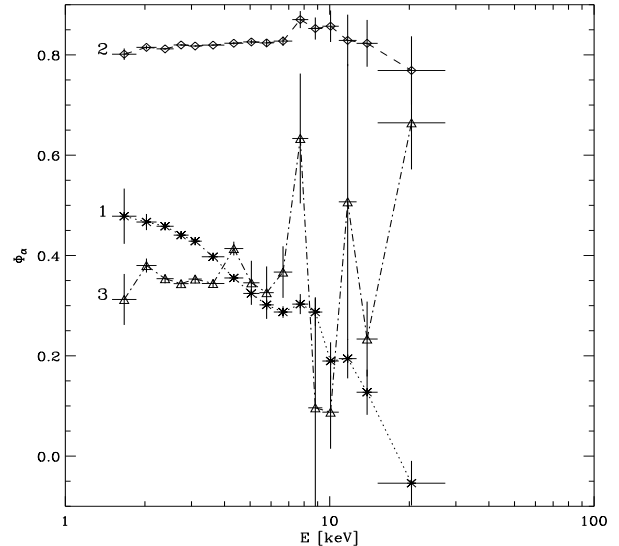


FIG. 9.— Phase angles as a function of energy for the first 3 harmonics used in the truncated Fourier series fit of the RXTE PCA pulse profiles of 1E 2259+586. Note that the position of the phase angle of the dominant second harmonic (labelled 2) is more or less constant (energy independent), while that of the first harmonic (labelled 1) decreases with increasing energy (shifts to the right).

Employing the same counts-extraction technique as used above for the other AXPs, the pulsed excess counts from the PCA profiles are converted into flux values taking into account the different PCU exposures and sensitivities, and adopting an absorbing Hydrogen column of $N_H = (9.3 \pm 0.3) \times 10^{21} \text{ cm}^{-2}$ (Patel et al. 2001).

Assuming a simple absorbed power-law model the fit resulted in a poor χ^2 of 26.24 for 14–2 degrees of freedom ($\chi_r^2 = 2.187$), indicating an inappropriate fitting function (there is a $\sim 1\%$ probability that such a high value of χ_r^2 is obtained at random assuming that the fit function is a good representation of the unknown parent function). An absorbed double power-law model, however, yielded a reasonable χ^2 of 16.70 for 14–4 degrees of freedom ($\sim 10\%$ random probability). The improvement $\Delta\chi^2$ of 9.55 adding two additional fit parameters translates to a $\sim 3\sigma$ improvement adopting a maximum likelihood ratio test. Thus, the double power-law model provided a significant improvement in describing the same spectral data. Adopting this double-power-law model as underlying photon model spectrum, the pulsed flux values are shown in Fig. 10 as aqua colored filled circles, and the best fit double-power-law model as a dashed aqua colored line.

The soft and hard power-law indices are $\Gamma_1 = 4.26 \pm 0.01$ and $\Gamma_2 = -1.02^{+0.24}_{-0.13}$, respectively, and the power-law-model components become equally strong at $E_{int} = 15.8 \pm 2.3$ keV. Thus, also for this AXP we witness the onset of a dramatic hardening of the pulsed spectrum beyond ~ 10 keV, although confirmation for energies beyond 20 keV is required. For HEXTE the source is too weak to be detected; 2σ upper limits (dark blue) are shown in Fig. 10.

6.2.2. Discussion of spectra and pulsed fractions of 1E 2259+586

The ISGRI flux upper limits to the total emission from 1E 2259+586 for energies above 20 keV (den Hartog et al. 2006) can be directly compared with the Chandra ACIS spectrum for

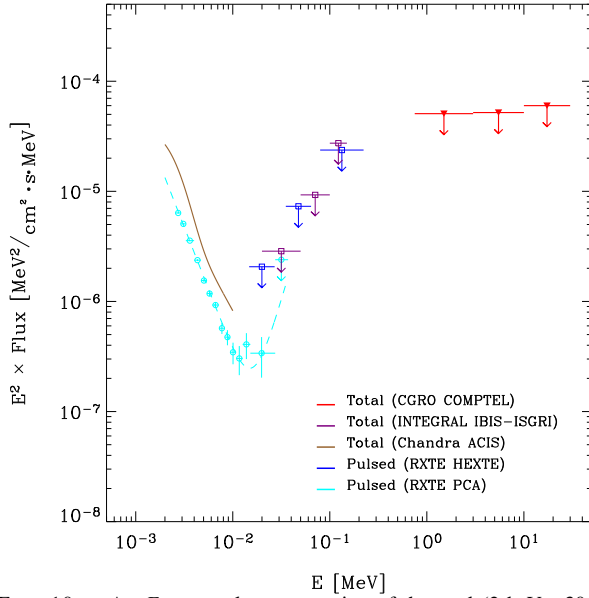


FIG. 10.— A νF_ν spectral representation of the total (2 keV - 30 MeV) and pulsed (2-30 keV) high-energy emission from 1E 2259+586. The dashed aqua coloured line represents the double power-law fit to the PCA 2-30 keV pulsed spectrum. This fit suggests the onset of a hard spectral tail in the pulsed spectrum near ~ 15 keV.

the 2-10 keV range. The black-body plus power-law model fit to this spectrum (Patel et al. 2001) is shown in Fig. 10 (dark-orange solid line). The double-power-law spectral fit suggests that again a minimum in luminosity is reached around 20 keV, where the extrapolation of the Chandra model fit crosses the pulsed PCA spectrum. Given the hard pulsed component suggested in these PCA data up to ~ 24 keV, we estimate that the source will show up at higher energies in an IBIS ISGRI mosaic totalling $\gtrsim 4$ Ms in effective on-axis exposure, what will be reached when adding in follow-up work already performed and/or scheduled observations. To complete the high-energy picture, the COMPTEL 0.75-30 MeV upper limits to the total emission (den Hartog et al. 2006) are also included in Fig. 10.

Comparing in the overlapping energy range below 10 keV the PCA time-averaged pulsed fluxes with the Chandra total emission model, and assuming no time variability, indicates a rather high value of $\gtrsim 43\%$ for the pulsed fraction (pulsed/total emission), in agreement with earlier estimates (Patel et al. 2001).

7. 1E 1048.1 - 5937

1E 1048.1 - 5937 was discovered with *Einstein* at an angular separation of $\sim 40'$ from η Car (Seward & Chlebowsky 1982). During an observation on July 13, 1979 a sinusoidally shaped signal with a high pulsed fraction of $68 \pm 7\%$ was detected at a period of ~ 6.44 s (Seward & Charles 1984; Seward et al. 1986). The pulsations at a period of 6.4407(9) s were confirmed in EXOSAT ME observations (Smale et al. 1985; Seward et al. 1986), and the positional accuracy of 1E 1048.1 - 5937 was further tightened up down to a radius of about $10''$.

Ginga observations combined with earlier measurements revealed a steady increase in spin period at a mean rate of $\dot{P} = (4.64 \pm 1.1) \times 10^{-4} \text{ s yr}^{-1}$ (Corbet & Day 1990), implying a rotational energy loss much smaller than the lower limit on the X-ray luminosity.

X-ray observations in the early nineties by ROSAT and ASCA

(Mereghetti 1995; Corbet & Mihara 1997) indicated that the spin-down rate almost doubled after 1988, likely anticorrelated with the X-ray flux.

BeppoSAX LECS / MECS data from long exposures in May 1997 indicated the necessity of a two component spectral model, a power-law plus black body, to describe properly the measured X-ray (0.5-10 keV) spectrum (Oosterbroek et al. 1998). This was confirmed by Paul et al. (2000) using ASCA data. In the meantime, detailed timing studies using RXTE monitoring observations performed in 1997-2000 (Kaspi et al. 2001) showed that significant deviations from simple spin-down exist, making phase-coherent timing impossible over time stretches longer than a few months. In spite of these rotational irregularities, neither pulse profile changes nor large pulsed flux variations were found. 1E 1048.1 - 5937 exhibited three X-ray bursts, on 2001 Oct. 29, 2001 Nov. 14, and 2004 June 29, all caught during RXTE monitoring observations (Gavril et al. 2002b, 2006).

Precise X-ray imaging of 1E 1048.1 - 5937 with Chandra (Wang & Chakrabarty 2002; Israel et al. 2002) provided a source position with sub-arcsecond accuracy. Within the $0''.7$ error circle only one faint near-IR source was found which clearly showed variability. A detailed variability study in the infrared and optical was undertaken by Durant & van Kerkwijk (2005). They established the variable nature in the infrared and optical and found a possible anticorrelation with the X-ray pulsed flux (see Gavril & Kaspi 2004, for an extensive study of the X-ray pulsed flux variability and spin-down rate variations). At radio

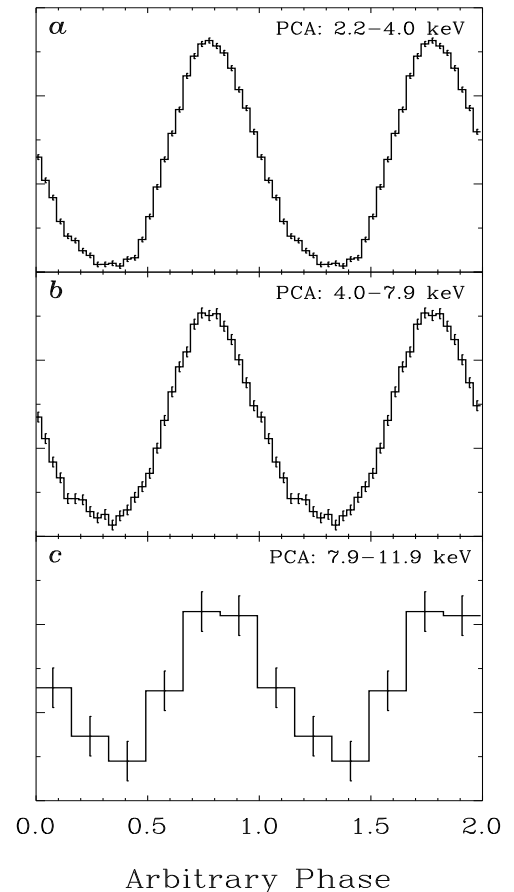


FIG. 11.— RXTE PCA pulse profiles of 1E 1048.1 - 5937 for energies in the range 2.2-11.9 keV combining data collected between July 27, 1996 and Feb. 24, 2004 (see Table 1). Two cycles are shown for clarity.

frequencies (21 cm) an expanding hydrogen shell centered on 1E 1048.1-5937 was detected (Gaensler et al. 2005), which can be interpreted as a wind bubble blown by a 30-40 M_{\odot} star, likely the massive progenitor of 1E 1048.1-5937.

Finally, the large effective area of XMM Newton, combined with accurate imaging, made it possible to perform in-depth (phase-resolved) spectral analyses not polluted by effects caused by the presence of strong nearby X-ray sources. XMM observed 1E 1048.1-5937 on three occasions and results are presented by Tiengo et al. (2002); Mereghetti et al. (2004) and Tiengo et al. (2005). Comparing the three XMM observations revealed long-term flux and pulsed fraction variations in anti-correlation. The featureless spectral shape, however, remained more or less the same, and could be described by a combination of a power-law with photon index $\Gamma \sim 2.7-3.5$ and a blackbody with temperature $kT \sim 0.63$ keV. Phase-resolved spectroscopy clearly indicated that the spectrum is softer at pulse minimum and harder at pulse maximum with respect to the phase averaged spectrum.

In the next section we present for the first time the hard X-ray/soft γ -ray timing and spectral characteristics of 1E 1048.1-5937 above ~ 8 keV using a) all available public RXTE PCA and HEXTE data (see Table 1), b) INTEGRAL IBIS ISGRI data (see Table 2) and c) CGRO COMPTEL 0.75-30 MeV data.

7.1. 1E 1048.1-5937 timing characteristics

In the timing analysis of the full set of PCA observations of 1E 1048.1-5937 listed in Table 1 according to the guidelines given in Sect. 3.1, we produced *time-averaged* pulse-phase distributions for energies between ~ 2 and 35 keV. In the folding/correlation process (see Sect. 3.1) we used the ephemerides given by Kaspi et al. (2001). Significant pulsed emission has been detected up to ~ 12 keV. The PCA pulse profiles of 1E 1048.1-5937 are shown in Fig. 11 for the three following differential energy bands, 2.2-4.0, 4.0-7.9 and 7.9-11.9 keV. The detection of pulsed emission, with a non-uniformity significance of 6.8σ , between ~ 7.9 and 11.9 keV is reported for the first time. The single peaked pulse profiles, with a slightly steeper rise than fall, do not show morphology changes as a function of energy. HEXTE data do not show pulsed emission at energies above ~ 15 keV.

7.2. 1E 1048.1-5937 spectral characteristics

7.2.1. RXTE PCA/HEXTE pulsed spectrum

The derived pulsed excess counts have been converted to flux values assuming an absorbing column density of $N_H = 1.0 \times 10^{22} \text{ cm}^{-2}$ (see Tiengo et al. 2005). It turned out that a single power-law model for the PCA band did not give an acceptable fit. Therefore we used for this AXP a black body plus power-law input spectrum. The optimized model ($\chi_r^2 = 0.55$ for 16 - 4 d.o.f.; $kT = 0.717(4)$ keV and $\Gamma = 2.93(7)$) is shown in Fig. 12 together with the flux measurements, both aqua colored. It is interesting to note, that, while the photon index is in the expected range (Tiengo et al. 2005), the (time-averaged) black body temperature of the pulsed component is slightly higher than the values obtained from the other X-ray instruments. This is very likely caused by the lack of sensitivity of the PCA for energies less than ~ 2.5 keV, thus poorly constraining the black body model at energies below its maximum. For HEXTE we could only derive upper limits for the pulsed emission, also shown in Fig. 12 as blue symbols.

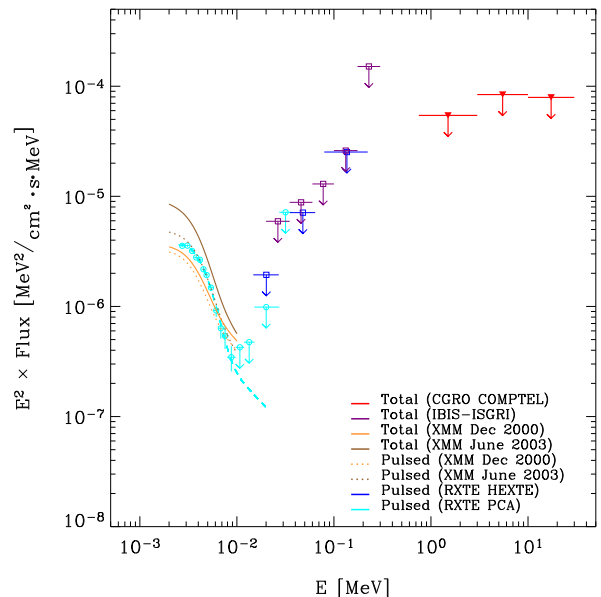


FIG. 12.— A νF_{ν} representation of the spectrum of 1E 1048.1-5937. Above ~ 12 keV the source is too weak to be detected so far. The IBIS ISGRI (purple) and CGRO COMPTEL (red) 2σ upper-limits are for the total emission. Below 10 keV we also added spectral information for the pulsed (dotted) and total (solid) emission from two XMM Newton observations performed at different epochs (Tiengo et al. 2005), illustrating the variable nature both in normalization and shape of both components.

7.2.2. INTEGRAL IBIS ISGRI and CGRO COMPTEL total spectrum

IBIS ISGRI data (Core program – GPS or public) from observations executed between revolution 30 and 217, satisfying our off-source pointing constraint of $14.5'$ have been used to obtain spectral information on the total emission from 1E 1048.1-5937 in the 20 – 300 keV energy range. The effective on-axis exposure time is, however, small ~ 250.8 ks, resulting in rather high upper-limits given the non-detections in any of the chosen broad energy bands. These 2σ upper-limits have been included in Fig.12 as purple symbols. Also, the analysis of full mission COMPTEL data (4.8 Ms exposure in total) did not result in significant detections of 1E 1048.1-5937. The 2σ COMPTEL upper-limits are shown as red symbols in Fig.12. It is clear from the full high-energy spectral picture presented in Fig. 12 that current spectral information above ~ 10 keV does not exclude the presence of a hard spectral component. Additional IBIS ISGRI data e.g. from a deep 2 Ms observation of the Carina region, performed between INTEGRAL revolutions 192 and 203, with 1E 1048.1-5937 always in the FCFOV, will be very useful to constrain the spectral properties of 1E 1048.1-5937 further in a future study.

8. 1E 1841-045

1E 1841-045 is the first AXP for which surprisingly non-thermal pulsed X-ray/soft γ -ray emission was discovered (Kuiper et al. 2004); see this paper also for a summary of earlier observational results on 1E 1841-045). The pulsed spectrum above 10 keV could be described, fitting RXTE PCA and HEXTE data, by a power-law model with photon index 0.94 ± 0.16 up to ~ 150 keV. The total spectrum of 1E 1841-045 presented in Kuiper et al. (2004) was derived from HEXTE data using source ON/OFF rocking-mode observations. We realized later

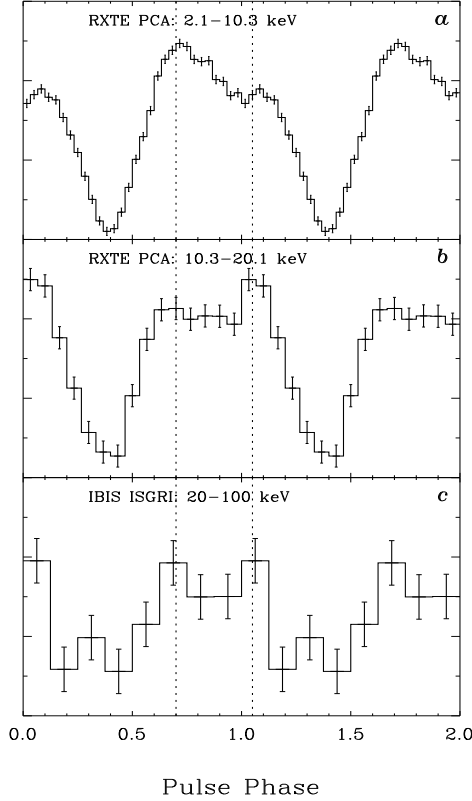


FIG. 13.— RXTE PCA pulse profiles of 1E 1841-045 for the 2.1-10.3 and 10.3-20.1 keV energy ranges (panels a and b, respectively), compared with the IBIS ISGRI 20-100 keV pulse profile (panel c). The dotted lines at phases 0.7 and 1.05 serve as a guide to the eye for alignment comparison purposes. The 20-100 keV IBIS ISGRI profile mimics the 10.3-20.1 keV RXTE PCA profile, suggesting a smooth prolongation above 20 keV of the 10.3-20.1 keV profile shape.

that the HEXTE flux values were contaminated by a contribution from the Galactic diffuse X-ray emission (see discussion in section 3.2). Better spectral information can be obtained with an imaging instrument like INTEGRAL IBIS ISGRI. Preliminary total flux measurements with ISGRI were so far only reported by Molkov et al. (2004). For the present work significantly more ISGRI data are available. Therefore, we present in this section a) a new spectrum of the total emission and b) performed now also a timing analysis for 1E 1841-045 using ISGRI data. Furthermore, c) we repeated the timing/spectral RXTE PCA analysis using additional data compared to Kuiper et al. (2004) as well as improved event selection criteria (see Sect. 3.1). Finally, d) also for this source we analyzed COMPTEL sky maps.

8.1. 1E 1841-045 pulse profiles for RXTE PCA and INTEGRAL IBIS ISGRI

In our RXTE reanalysis for 1E 1841-045, data from observation 80098 (spread over 28-3-2003 – 17-2-2004; screened PCU-2 exposure ~ 69.1 ks) were added to the set used in Kuiper et al. (2004) (now, total screened PCU-2 exposure: ~ 340.2 ks). We used in the folding/correlation process (see Sect. 3.1) the ephemerides given by Gotthelf et al. (2002) and derived in this work (see Table 3). The results are pulse profiles with improved statistics, confirming the variation of pulse shape with energy as presented by (Kuiper et al. 2004). As an example, Fig. 13

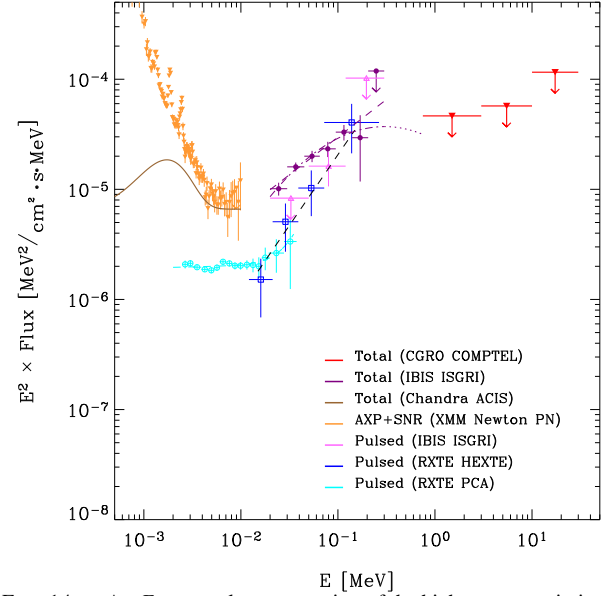


FIG. 14.— A νF_ν spectral representation of the high-energy emission from 1E 1841-045 and SNR Kes 73. The aqua, blue and magenta data points/curves represent the (time averaged) pulsed emission component of the spectrum (2-300 keV) based on RXTE PCA/HEXTE and INTEGRAL IBIS ISGRI observations. The black dashed line shows the best power-law model fit to the PCA, HEXTE and ISGRI pulsed flux values for energies above ~ 15 keV. The purple data points/curves reflect the IBIS ISGRI total flux measurements and fits (power-law, dashed; curved power-law, dashed-dotted and extrapolated to 750 keV). The red 2σ upper limits from CGRO COMPTEL require a spectral break, somewhere between 140 and 750 keV. For completeness, below 10 keV also the total flux from 1E 1841-045 plus SNR Kes 73 (yellow symbols; XMM Newton) and the total flux from 1E 1841-045 (dark orange solid line; Chandra ACIS) are shown (see Kuiper et al. 2004, for more details).

(panels a and b) shows RXTE PCA profiles for the 2.1-10.3 and 10.3-20.1 keV energy bands.

IBIS ISGRI data from observations with source off-axis angles less than $\leq 14.5^\circ$ and taken during INTEGRAL revolutions 49 - 123 have been processed to yield pulse phase distributions for differential energy bands between 20 and 300 keV. The total screened effective on-axis exposure was ~ 808.8 ks. We derived a very accurate (RMS residual is 0.015 in phase; see Table 3 for the details) phase coherent ephemeris using RXTE PCA monitoring observations performed during March - December 2003. This has been applied in the folding process of the selected barycentered ISGRI events. For the 20-100 keV energy range we obtained a Z_2^2 of 3.6σ . This ISGRI pulse profile is also shown in Fig. 13 (panel c). Its shape mimics that of the PCA 10.3-20.1 keV profile suggesting a stable pulse shape in the hard X-ray window. The statistics are still low, however, but additional ISGRI data from already performed and future scheduled observations will allow more detailed studies of the pulse shape in this energy range.

8.2. 1E 1841-045 spectral characteristics

8.2.1. RXTE and INTEGRAL pulsed emission

Starting with the new RXTE PCA phase distributions, introduced above, the updated 1E 1841-045 pulsed spectrum, now with significant flux values up to ~ 28 keV, is shown in Fig. 14 using aqua colored symbols. Also given are the earlier-reported pulsed-flux values from HEXTE (dark blue data points; see Kuiper et al. 2004), which clearly revealed the hard pulsed component up to ~ 150 keV.

Now we can also derive information on the pulsed spectrum from IBIS ISGRI. Phase distributions have been generated, followed by extraction of pulsed counts, for three logarithmically spaced energy bands (20-50, 50-120 and 120-300 keV), yielding only for the 50-120 keV band a significant pulsed-flux measurement. This ISGRI pulsed-flux value and two upper limits, shown in Fig. 14 as magenta symbols, are fully consistent with the hard spectrum measured by HEXTE. We fitted the new PCA pulsed spectrum for energies above ~ 15 keV together with the HEXTE and INTEGRAL pulsed flux data points with a simple power-law model, yielding as best fit a photon index Γ of 0.72 ± 0.15 , slightly harder than derived by Kuiper et al. (2004). This best fit model is indicated as a dashed black line in Fig. 14.

8.2.2. INTEGRAL total emission

In this work we derived the total emission spectrum of 1E 1841-045 in the 20-300 keV energy range from IBIS ISGRI mosaic maps generated for 7 differential energy bands over the 20 - 300 keV band, thus significantly improving upon the spectral information given by Molkov et al. (2004). We used a combination of public and Core program observations, all with source off-pointing angles less than $14^\circ 5$, and for which the details⁶ are listed in Table 2. The total screened effective on-axis exposure on 1E 1841-045 in this combination was $\sim 1,111$ Ms. Significant emission has been detected up to ~ 140 keV ($95-140$ keV; 5.7 ± 0.9 mCrab). The derived flux values are shown in Fig. 14 as purple colored symbols. Over this 20-300 keV band we can *not* discriminate between a power-law or power-law model with energy dependent index to be the best model describing the measurements. However, including in Fig. 14 the CGRO COMPTEL flux upper limits (red symbols) derived in this work, we notice that the best fitting power-law model with photon index $\Gamma = 1.32 \pm 0.11$ does not extend into the MeV domain. The spectrum must break somewhere between 140 and 750 keV. The curved power-law model is consistent with the COMPTEL 2σ upper limits. Both models are shown in Fig. 14 as purple dashed (power-law) and purple dashed-dotted (curved power-law) lines with the latter model extrapolated up to 750 keV.

8.2.3. Discussion of spectra and pulsed fractions of 1E 1841-045

The new and better total spectrum of 1E 1841-045, now derived using ISGRI data, is indeed lower, ~ 40 % between 20 and 100 keV, than published earlier using HEXTE data (Kuiper et al. 2004), and is also slightly harder. It connects better to the total spectra measured at different epochs by XMM Newton and Chandra ACIS below 10 keV, shown in Fig. 14 and adopted from Kuiper et al. (2004, and citations therein).

For the pulsed spectrum, the power-law fit to the new PCA spectrum above ~ 15 keV combined with the new ISGRI measurements and the earlier published HEXTE flux values, confirms the drastic up turn/hardening of the pulsed spectrum. Also, the extrapolation of this very hard spectrum has to remain under our COMPTEL upper limits, requiring an even more drastic bend/break compared to what is required for the total spectrum.

The compilation of Chandra, XMM-Newton, RXTE and INTEGRAL spectra in Fig. 14, taken at very different epochs over many years, suggests that the hard X-ray emission of 1E

1841-045 is stable, i.e. this magnetar is most of the time in the same state of activity for energies above ~ 10 keV. The pulsed fraction is confirmed to be $\sim 25\%$ at 20 keV and $\sim 100\%$ for energies beyond ~ 100 keV.

9. SUMMARY

Exploiting the availability of archival data from RXTE monitoring observations and new, deep INTEGRAL exposures of AXPs, we were able to show that AXPs exhibit exceptionally hard spectra for energies above 10 keV. Of the sample of five AXPs studied in this work, three (the brightest at energies below 10 keV: 1E 1841-045, 1RXS J1708-4009, 4U 0142+61) are shown to emit up to energies of ~ 150 keV. Of the two weaker sources, for one (1E 2259+586) an upturn of pulsed emission is suggested up to ~ 25 keV, and the other (1E 1048.1-5937) is too weak to detect a possible similar upturn in the hard-X-ray range with presently available exposures. We regard this sufficient evidence to conclude that a persistent non-thermal component at energies above 10 keV is a common property of AXPs.

In Table 4 we summarize for the five AXPs the spectral parameters presented in this work, together with estimates for their distances and pulsar characteristics (period, period derivative, deduced surface magnetic field strength at the pole and spin-down power). Most interesting and new are the results on the total and pulsed spectra, and luminosities above 10 keV. As noted above, the exceptionally hard pulsed spectra seem to extend up to at least 150 keV, therefore we have given for all four AXPs for which the spectral up turn around 10 keV has been measured, the luminosity of the pulsed component integrating the best-fit power-law model over the full decade in energy from 10 to 100 keV. For the luminosity of the pulsed component between 1 and 10 keV, we list the power in the power-law component fitted to the pulsed spectra before the break, except for 1E 1048.1-5937, where the power has been derived from a black body plus power-law model. Thus for 4 AXPs we ignore the presence of a black-body component which is known to be present at lower energies as well. However, for 1RXS J1708-4009, 4U 0142+61, 1E 2259+586 and 1E 1841-045 we could fit the pulsed PCA spectra down to about 2 keV well with a single power-law model.

The total spectra above 20 keV appear also to be hard, but somewhat softer than the pulsed spectra.

For 1E 1841-045 and 4U 0142+61 the total emission becomes consistent with 100% pulsed around ~ 100 keV, starting from a pulsed fraction at 10 keV of $\sim 25\%$ and $\sim 10\%$ for 1E 1841-045 and 4U 0142+61, respectively. The exception is 1RXS J1708-4009, for which the hard X-ray emission above 10 keV is consistent with being 100% pulsed. Note in this context, however, the strong intensity variability reported for this AXP for energies below 10 keV, which might be coupled to variations in pulsed fraction.

Table 4 immediately shows that the luminosities of the hard X-ray components (pulsed and total) exceed the available total spin-down powers by a few orders of magnitude, a conclusion drawn earlier for the total luminosities (black body plus power-law components) in the 1 – 10 keV band.

Our compilations of total and pulsed flux values for energies above 10 keV for the three strongest AXPs, using data from different instruments and collected at different epochs, suggest that the high-energy component is stable, contrary to reports for the emissions below 10 keV. However, additional observations

⁶ Data from Revs. 131,133-134 were ignored because these have been taken in a staring mode configuration giving rise to substantial systematical effects in the image deconvolution procedures.

TABLE 4

PULSAR CHARACTERISTICS AND HIGH-ENERGY SPECTRAL PROPERTIES (PULSED/TOTAL) OF THE AXPs STUDIED IN THIS WORK.

AXP	P s	\dot{P} 10^{-11} s/s	B_s 10^{14} G	L_{sd}^{32} erg/s	d kpc	$L_{1-10}^{32,p}$ erg/s	Γ_l^p	$L_{10-100}^{32,p}$ erg/s	Γ_h^p	$L_{10-100}^{32,l}$ erg/s	Γ_h^l
1E 1841-045	11.78	4.44	7.32	10.73	6.7	391	1.98(2)	1312	0.72(15)	2975	1.32(11)
1RXS J1708-4009	11.00	1.92	4.64	5.68	5	640	2.60(1)	719	1.01(12)	869	1.44(45)
4U 0142+61	8.69	0.20	1.34	1.21	3	347	4.09(2)	686 [†]	-0.80(9) [†]	638	1.05(11)
1E 2259+586	6.98	0.048	0.59	0.56	3	485	4.26(1)	188 [†]	-1.02(19) [†]
1E 1048.1-5937	6.45	2.31	3.90	33.90	2.7	76*	*

[†] Based on double power-law fit to PCA data (~ 2 -30 keV); 30-100 keV luminosity extrapolated from this model

* The 1-10 keV luminosity has been derived from a black body plus power-law model fit

 L^{32} means that the luminosity is expressed in units 10^{32} erg/s

are required (and will become available with INTEGRAL) to constrain this further.

The time-averaged light curves for the different AXPs suggest that the pulse shapes for energies above 10 keV exhibit less structure, and vary less with energy than seen below 10 keV. However, the statistics are still insufficient to draw stringent conclusions. Phase-resolved spectroscopy on time-averaged profiles will be performed when more INTEGRAL data can be added.

10. DISCUSSION

The discussion of AXPs in the context of magnetically powered rotating neutron stars, was till recently focussed on understanding the observational characteristics of the soft-spectrum component for energies below 10 keV. Indeed, evidence for hard X-ray or soft gamma-ray emission from AXPs was lacking, in contrast to the very luminous outbursts at soft gamma-ray energies characterizing SGRs. Our discovery of pulsed emission from AXPs up to at least ~ 150 keV adds a completely new non-thermal component requiring a steady mechanism for accelerating particles in magnetospheres of magnetars. Also this new quiescent emission component is far too luminous to be powered by rotational energy loss, as is evident in Table 4. Recently, INTEGRAL also found for the first time quiescent hard X-ray emission from a SGR (SGR 1806-20; Molokov et al. 2005; Mereghetti et al. 2005). As for AXPs, its spectrum above 10 keV could be fitted with a hard power-law model, photon index 1.6 ± 0.1 , an index comparable to, but somewhat softer than that measured for the total AXP spectra in that energy window, but significantly softer than the hard spectra reported in this work for the quiescent pulsed spectra of AXPs. In addition, the quiescent SGR spectrum does not exhibit a black body component at energies below 10 keV. This underlines again, that AXPs and SGRs are (very) different manifestations of the magnetar scenario.

In Table 4, we listed the high-energy characteristics for five AXPs studied in this work, out of a total of six persistent AXPs known to date. Although this sample is still very small, we verified whether there are already any apparent correlations between the measured parameters. There is a hint for a correlation between the magnetic field strength B_s and the luminosity L_{10-100}^p of the pulsed emission of the hard tail (10-100 keV) for four AXPs, as well as the total emission of the hard tail (now for three AXPs). However, 1E 1048.1-5937 has a B_s three times higher than 4U 0142+61, and is located at a similar distance, but no hard X-ray emission has been detected, and its luminosity at ~ 10 keV is about three times lower than that of 4U 0142+61. It is interesting to note that the spin down lumi-

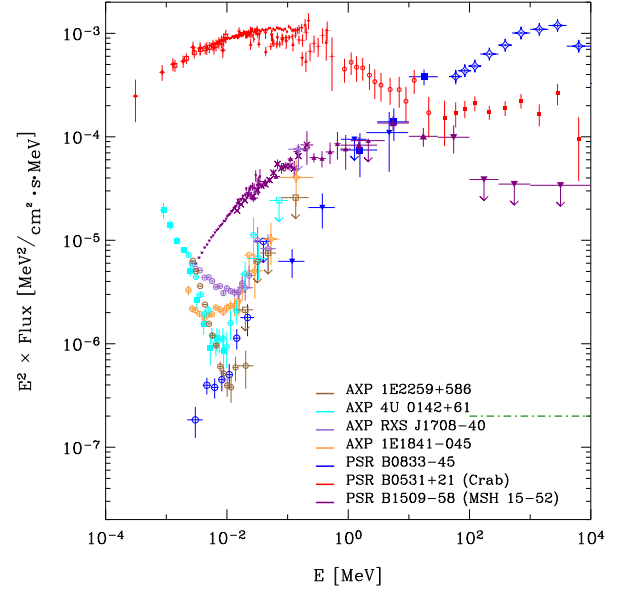


FIG. 15.— A νF_ν spectral representation of the pulsed emission for the 4 AXPs showing hard spectral tails. For comparison purposes, also the pulsed high-energy (~ 1 keV - 10 GeV) spectra of the young Crab (PSR B0531+21) and PSR B1509-58 pulsars, and the middle-aged Vela pulsar (PSR B0833-045) are shown. Furthermore, the 3σ GLAST sensitivity (green dashed-dotted line) assuming an E^{-2} source for an all-sky survey duration of one year (> 100 MeV) is shown.

nosity of 1E 1048.1-5937 is the highest of this sample, mainly due to its large \dot{P} , and reaches almost 50% of the luminosity of the pulsed emission between 1 and 10 keV, a factor 10 - 100 higher than for the other four AXPs.

Surprisingly, the high-energy AXP spectra are very similar to those of "middle-aged" radio pulsars in the ~ 10 -300 keV energy band. This can be seen in Fig. 15 in which the AXP spectra are shown together with the spectra of two young radio pulsars, PSR B0531+21 (Crab) and PSR B1509-58, and the middle-aged Vela pulsar (PSR B0833-45). These are the only radio pulsars which have been detected from soft X-rays up to the gamma-ray domain. The other middle-aged high-energy gamma-ray pulsars detected by CGRO EGRET (see e.g. the review by Thompson et al. 1997) are detected at high-energy gamma-rays (> 100 MeV), and soft X-rays, but not in the intermediate hard X-ray range, in which they are weaker than the Vela pulsar. The overall high-energy spectral shape of these middle-aged pulsars is expected to be similar to that of Vela. Like the AXPs, the Vela pulsar has a (pulsed) thermal black-body component (only visible below 2 keV, and not shown in

Fig. 15), and an extrapolation of its power-law shape spectrum above 10 keV to the IR, optical and radio domains is approximately in agreement with the measured flux values at these longer wavelengths. This is rather similar to the case of e.g. AXP 4U 0142+61, with the difference that none of the AXPs have so far been seen in the radio, and the X-ray and IR emissions exhibit a time variable behaviour, not seen for Vela. This similarity of the multiwavelengths spectra could suggest some similarity in production processes in the two different scenarios of rotation-powered pulsars and magnetars starting from very different sources of power.

A first attempt, before our discovery of hard X-ray emission from AXPs, to model possible production of high-energy (X-ray and gamma-ray) emission in the magnetospheres of AXPs, applying a scenario proposed for high-energy production in the magnetospheres of radio pulsars, was made by Cheng & Zhang (2001). They modeled the production of high-energy (above 100 MeV) gamma-radiation in outer magnetospheric gaps of AXPs. They argued that due to the strong field of a magnetar, the gamma-ray emission rooted at the polar caps will be quenched. However, far away from the pulsar surface, i.e. in outer vacuum gaps, gamma radiation could be emitted because the local field will drop below the critical quantum limit. They predict that the NASA Gamma-ray Large Area Space Telescope GLAST, due for launch in 2007, might be able to detect this very-high-energy emission from AXPs (see Fig. 15 for the 3σ GLAST sensitivity assuming an E^{-2} source spectrum for an all-sky survey duration of one year). However, their model calculations do not reproduce the hard spectra and high X-ray luminosities now discovered above 10 keV.

The publication of the discovery of a hard spectral tail of 1E 1841-045 by Kuiper et al. (2004) stimulated Thompson & Beloborodov (2005) to reconsider high-energy emission from magnetars due to an ultra strong magnetic field. A gradual release of energy in the stellar magnetosphere is expected if it is twisted and a strong electric current is induced on the closed field lines. They considered two mechanisms of gamma-ray emission:

(1) A thin surface layer of the star is heated by the downward beam of current carrying charges, which excite Langmuir turbulence in the layer. Thus, a temperature kT of ~ 100 keV can be reached, emitting bremsstrahlung photons up to this characteristic temperature. Interestingly, three of the AXPs, 1RXS J1708-4009, 4U 0142+61 and 1E 1841-045, were detected up to these energies of ~ 150 keV, the shapes of their total and/or pulsed spectra being consistent with this mechanism with peak luminosities around the predicted energy. However, the 100% pulsed fraction around 20 keV for 1RXS J1708-4009 is difficult to reconcile with the surface emission, given the effects of general relativistic light bending. Future observations have to reveal whether the cut off in the spectra is also consistent with this interpretation.

(2) Soft γ -rays are produced at a distance of ~ 100 km from the star surface in the magnetosphere, where the electron cyclotron energy is in the keV range. A large electric field develops in this region in response to the outward drag force felt by the current-carrying electrons from the flux of keV photons leaving the star. Thompson & Beloborodov show that a seed photon injected in this region undergoes a runaway acceleration and upscatters keV photons above the threshold for pair creation. The resulting synchrotron spectrum can reach a peak at ~ 1 MeV. Our hard-X-ray spectra together with the upper

limits from COMPTEL in the MeV domain, allow spectra with maximum luminosities close to the MeV range. But we should note that the flux values reported around ~ 100 keV are already at about the same level as the $2\text{-}\sigma$ upper limits for the 0.75–3 MeV interval, suggesting a different shape, thus challenging this interpretation.

An alternative quantum-electrodynamics model for the bursts and the quiescent non-thermal emission from AXPs as well as SGRs was proposed by Heyl & Hernquist (2005a,b). Their model is based on fast-mode breakdown, in which wave energy is dissipated into electron-positron pairs when the scale of these discontinuities becomes comparable to an electron Compton wavelength. They showed that under appropriate conditions, an electron-positron fireball would result, producing primarily the X-ray and soft-gamma-ray bursts. They also investigated (Heyl & Hernquist 2005b) the properties of non-thermal emission in the absence of a fire ball. This quiescent, non-thermal emission associated with fast-mode breakdown may account for the observed non-thermal emission presented in this work for AXPs, as well as for the quiescent emission reported for SGR 1806-20 (Molkov et al. 2005; Mereghetti et al. 2005). Indeed, they succeeded in fitting ISGRI AXP spectra as well as unabsorbed optical data for 4U 0142+61 from Hulleman et al. (2000), and the SGR 1806-20 non-thermal spectrum above 10 keV. Interestingly, they predict that the emission should extend beyond the observed INTEGRAL spectra without a break below 1 MeV. However, the combination of ISGRI spectra and COMPTEL upper limits presented in this work, seem to contradict this claim. They further state, that if the magnetars have significant optical excesses, such as 4U 0142+61, then the quiescent emission from most of the AXPs discussed in this work and of SGR 1806-20 should be detectable with GLAST (see again Fig. 15 for the GLAST sensitivity). Further INTEGRAL observations, and ultimately GLAST observations can support or reject these claims.

Over the last few years, two radio pulsars with periods and period time derivatives similar to those found for AXPs, thus also with high-magnetic-field strengths, are found: PSR J1847-0130, which has the highest by far inferred surface dipolar magnetic field ($B = 9.4 \times 10^{13}$ G) among all known radio pulsars (McLaughlin et al. 2003) and PSR J1718-3718 (Hobbs et al. 2004; Kaspi & McLaughlin 2005). The X-ray luminosities (or upper-limits to these) in the 2-10 keV range derived for these two radio pulsars are much lower than those of the standard AXP group. Above 10 keV, detection of hard X-rays could connect these two different types of neutron stars. PSR J1847-0130 and PSR J1718-3718 both happened to be located near the centers of our deep IBIS ISGRI exposures on 1E 1841-045 and 1RXS J1708-4009, respectively. Therefore, we searched above 20 keV for hard X-ray signatures from these pulsars, but nothing was detected in any of the energy bands we have investigated. The 2σ upper limit on the flux in the 20-30 keV band for PSR J1847-0130 is 0.4 mCrab⁷ and that for PSR J1718-3718 is also 0.4 mCrab, but now in the 20-35 keV band.

Therefore, why solitary rotating neutron stars with AXP-like timing parameters in some cases behave as “dull” radio pulsars and in other cases as “enigmatic” magnetars is still unclear. Different suggestions have been made (see e.g. McLaughlin et al. 2003), one of the possibilities being that high-field pulsars and AXPs have similar dipole magnetic fields, but AXPs have also quadrupole (or higher) components. Kaspi & McLaughlin

⁷ 1E 1841-045 is detected in the same image with a flux of $\sim 1.5 \pm 0.2$ mCrab

(2005) suggest a.o. the interesting possibility that the high-field radio pulsars, may one day emit transient magnetar-like emission, and conversely that the transient AXPs might be more likely to exhibit radio pulsations. More theoretical work is required, but certainly also more detailed observational results at all wavelengths to verify the model predictions. Ongoing observations of AXPs with the wide-field-of-view INTEGRAL IBIS imager will allow us to contribute with deeper studies in the hard X-ray/soft γ -ray range.

This research has made use of data obtained from the High Energy Astrophysics Science Archive Research Center (HEASARC), provided by NASA's Goddard Space Flight Center, and of data obtained through the INTEGRAL Science Data Centre (ISDC), Versoix, Switzerland. INTEGRAL is an ESA project with instruments and science data centre funded by ESA member states (especially the PI countries: Denmark, France, Germany, Italy, Switzerland, Spain), Czech Republic and Poland, and with the participation of Russia and the USA. We have extensively used NASA's Astrophysics Data System (ADS). We thank Anton Klumper and Jaap Schuurmans for the maintenance of the OSA software at SRON and the INTEGRAL data import from the ISDC site. Nanda Rea is acknowledged for useful discussions on AXPs in general. Finally, we appreciate the willingness of Jacco Vink and Maurizio Falanga to make their INTEGRAL open time data of the Cassiopeia region (Revs. 261-269) directly available for us.

REFERENCES

- Baykal, A., Strohmayer, T., Swank, J. 2000, MNRAS, 319, 205
- Bloemen, H., Hermesen, W., Swaneburg, B.N., et al. 1994, ApJS, 92, 419
- de Boer, H., Bennett, K., den Herder, J.W., et al. 1992, in DATA ANALYSIS IN ASTRONOMY - IV, 241
- Buccheri, R., Bennett, K., Bignami, G.F., et al. 1983, A&A, 128, 245
- Cheng, K.S. and Zhang, L. 2001, ApJ, 562, 918
- Coe, M.J., Jones, L.R., and Lehto, H. 1994, MNRAS, 270, 178
- Corbet, R.H.D. and Day, C.S.R. 1990, MNRAS, 243, 553
- Corbet, R.H.D., Smale, A.P., Ozaki, M., et al. 1995, ApJ, 443, 786
- Corbet, R.H.D. and Mihara, T. 1997, ApJ, 475, L127
- Courvoisier, T.J.-L., Walter, R., Beckmann, V., et al. 2003, A&A, 411, L53
- Durant, M. and van Kerkwijk, M. 2005, ApJ, 627, 376
- Dall'Osso, S., Israel, G.L., Stella, L., et al. 2003, ApJ, 599, 485
- Fahlman, G.G. and Gregory, P.C. 1981, Nature, 293, 202
- Fahlman, G.G. and Gregory, P.C. 1983, in Supernova Remnants and their X-Ray Emission,
- Falanga, M., Kuiper, L., Poutanen, J., et al. 2005, A&A, in press
- Forman, W., Jones, C., Cominsky, L., et al. 1978, ApJS, 38, 357
- Gaensler, B.M., Slane, P.O., Gotthelf, E.V., et al. 2001, ApJ, 559, 963
- Gaensler, B.M., McClure-Griffiths, N.M., Oey, M.S., et al. 2005, ApJ, 620, L95
- Gavriil, F.P. and Kaspi, V.M. 2002, ApJ, 567, 1067
- Gavriil, F.P., Kaspi, V.M., Woods, P.M. 2002, Nature, 419, 142
- Gavriil, F.P., Kaspi, V.M., Woods, P.M. 2004, ApJ, 607, 959
- Gavriil, F.P., Kaspi, V.M., Woods, P.M. 2005, astro-ph/0507047
- Gavriil, F.P. and Kaspi, V.M. 2004, ApJ, 609, L67
- Göhler, E., Wilms, J. and Staubert, R. 2005, A&A, 433, 1079
- Goldwurm, A., David, P., Foschini, L., et al. 2003, A&A, 411, L223
- Gotthelf, E.V., Gavriil, F.P., Kaspi, V.M., et al. 2002, ApJ, 564, L31
- Gregory, P.C. and Fahlman, G.G. 1980, Nature, 287, 805
- Gregory, P.C., Braun, R., Fahlman, G.G. et al. 1983, in Supernova Remnants and their X-Ray Emission, Proceedings of the IAU Symposium, Venice, Italy, August 30-September 2, 1982, eds. Danziger, J. and Gorenstein, P., 437-443
- Hanson, C.G., Dennerl, K., Coe, M.J., et al. 1988, A&A, 195, 114
- den Hartog, P.R., Kuiper, L., Hermesen, W., et al. 2004, ATEL 293
- den Hartog, P.R., Hermesen, W., Kuiper, L., et al. 2006, A&A in press
- Hellier, C., 1994, MNRAS, 271, L21
- Hobbs, G., et al. 2004, MNRAS, 352, 1439
- Hughes, V.A., Harten, R.H., Costain, C.H., et al. 1984, ApJ, 283, 147
- Hulleman, F., van Kerkwijk, M.H. and Kulkarni, S. 2000, Nature, 408, 689
- Hulleman, F., Tennant, A.F., van Kerkwijk, M.H. et al. 2001, ApJ, 563, L49
- Heyl, J.S. and Hernquist, L. 2005, ApJ, 618, 463
- Heyl, J.S. and Hernquist, L. 2005, MNRAS, 362, 777
- Israel, G.L., Mereghetti, S. and Stella, L. 1994, ApJ, 433, L25
- Israel, G.L., Covino, S., Stella, L., et al. 1999, ApJ, 518, L107
- Israel, G.L., Oosterbroek, T., Angelini, L. 1999, A&A, 346, 929
- Israel, G.L., Oosterbroek, T., Stella, L. 2001, ApJ, 560, L65
- Israel, G.L., Covino, S., Stella, L. 2002, ApJ, 580, L143
- Israel, G.L., Covino, S., Perna, R. 2003, ApJ, 589, L93
- Iwasawa, K., Koyama, K., and Halpern, J.P. 1992, PASJ, 44, 9
- Jahoda, K., Swank, J.H., Giles, A.B., et al. 1996, Proc. SPIE, 2808, 59
- Juett, A.M., Marshall, H.L., Chakrabarty, D., et al. 2002, ApJ, 568, L31
- Koyama, K., Hoshi, R. and Nagase, F. 1987, PASJ, 39, 801
- Koyama, K., Nagase, F., Ogawara, Y., et al. 1989, PASJ, 41, 461
- Kaspi V.M., Chakrabarty, D. and Steinberger, J. 1999, ApJ, 525, L33
- Kaspi V.M., Lackey, J.R. and Chakrabarty, D. 2000, ApJ, 537, L31
- Kaspi V.M., Gavriil, F.P., Chakrabarty, D., et al. 2001, ApJ, 558, 253
- Kaspi V.M. and Gavriil, F.P. 2003, ApJ, 596, L71
- Kaspi V.M., Gavriil, F.P., Woods, P.M., et al. 2003, ApJ, 588, L93
- Kaspi V.M. and McLaughlin, M.A. 2005, ApJ, 618, L41
- Kriss, G. A., Becker, R.H., Helfand, D.J., et al. 1985, ApJ, 288, 703
- Kuiper, L., Hermesen, W., Krijger, J.M., et al. 1999, A&A, 351, 119
- Kuiper, L., Hermesen, W., Cusumano, G., et al. 2001, A&A, 378, 918
- Kuiper, L., Hermesen, W., Walter, R., et al. 2003, A&A, 411, L31
- Kuiper, L., Hermesen, W., and Mendež, M. 2004, ApJ, 613, 1173
- Lebrun, F., Leray, J. P., Lavocat, P., et al. 2003, A&A, 411, L141
- McLaughlin, M.A., Stairs, I.H., Kaspi, V.M., et al. 2003, ApJ, 591, L135
- Mereghetti, S. 1995, ApJ, 455, 598
- Mereghetti, S., Israel, G.L., and Stella, L. 1998, MNRAS, 296, 689
- Mereghetti, S., Chialone, L., Israel, G.L., et al. 2002, Proc. 270 WE-Heraeus Seminar, 29
- Mereghetti, S., Tiengo, A., Stella, L., et al. 2004, ApJ, 608, 427
- Mereghetti, S., Götz, D., Mirabel, I.F., et al. 2005, A&A, 433, L9
- Morini, M., Robba, N.R., Smith, A., et al. 1988, ApJ, 333, 777
- Kern, B. and Martini, C. 2002, Nature, 417, 527
- Molkov, S.V., Cherepashchuk, A.M., Lutovinov, A.A., et al. 2004, Astronomy Letters, 30, 534
- Molkov, S.V., Hurley, K., Sunyaev, R., et al. 2005, A&A, 433, L13
- Mori, M., Kawai, N. and Shibazaki, N. 2005, ApJ, 622, 544
- Motch, C., Belloni, T., Buckley, D., et al. 1991, A&A, 246, L24
- Oosterbroek, T., Parmar, A.N., Mereghetti, S., et al. 1998, A&A, 334, 925
- Parmar, A.N., Oosterbroek, T., Favata, F., et al. 1998, A&A, 330, 175
- Patel, S.K., Kouveliotou, C., Woods, P.M., et al. 2001, ApJ, 563, L45
- Patel, S.K., Kouveliotou, C., Woods, P.M., et al. 2003, ApJ, 587, 367
- Paul, B., Kawasaki, M., Dotani, T., et al. 2000, ApJ, 537, 319
- de Plaa, J., Kuiper, L., Hermesen, W. 2003, A&A, 400, 1013
- Rea, N., Israel, G.L., Stella, L., et al. 2003, ApJ, 586, L65
- Rea, N., Oosterbroek, T., Zane, S., et al. 2005, MNRAS, 361, 710
- Rea, N., et al. 2006, in prep.
- Reid, C.A., Johnston, M.D., Bradt, H.V., et al. 1980, AJ, 85, 1062
- Revnivtsev, M. G., Sunyaev, R. A., Varshalovich, D. A., et al. 2004, Astronomy Letters, 30, 382
- Rho, J. and Petre, R. 1997, ApJ, 484, 828
- Rothschild, R.E., Blanco, P.R., Gruber, D.E., et al. 1998, ApJ, 496, 538
- Rots, A., Jahoda, K., and Lyne, A.G., 2004, ApJ, 605, L129
- Safi-Harb, S. & West, J. 2005, AdSpR, 35, 1172
- Schönfelder, V., Aarts, H., Bennett, K., et al. 1993, ApJS86, 657
- Seward, F.D. and Chlebowski, T. 1982, ApJ, 256, 530
- Seward, F.D. and Charles, P.A. 1984, BAAS, 16, 983
- Seward, F.D., Charles, P.A. and Smale, A.P. 1986, ApJ, 305, 814
- Smale, A.P., Charles, P.A., Corbet, R.H.D., et al. 1985, IAU Circ., 4083
- Sugizaki, M., Nagase, F., Torri, K., et al. 1997, PASJ, 49, L25
- Tam, C.R., Kaspi, V.M., van Kerkwijk, M.H., et al. 2004, ApJ, 617, L53
- Tiengo, A., G'ohler, E., Staubert, R., et al. 2002, A&A, 383, 182
- Tiengo, A., Mereghetti, S., Turolla, R., et al. 2005, A&A, 437, 997
- Thompson, C. and Duncan, R.C. 1996, ApJ, 473, 322
- Thompson, C. and Beloborodov, A.M. 2005, ApJ, 634, 565
- Thompson, D. J., Harding, A. K., Hermesen, W., et al. 1997, Proceedings of the Fourth Compton Symposium, Eds. Charles D. Dermer, Mark S. Strickman, and James D. Kurfess, Williamsburg, VA, April 1997: AIP Conference Proceedings 410, p. 39.
- Ubertini, P., Lebrun, F., Di Cocco, G., et al. 2003, A&A, 411, L131
- Valinia, A. and Marshall, F.E. 1998, ApJ, 505, 134
- Vedrenne, G., Roques, J.-P., Schönfelder, V., et al. 2003, A&A, 411, L63
- Wachter, S., Patel, S.K., Kouveliotou, C. 2004, ApJ, 615, 887
- Walter, R., Favre, P., Dubath, P., et al. 2003, A&A, 411, L25
- Wang, Z. and Chakrabarty, D. 2002, ApJ, 579, L33
- Warwick, R.S., Marshall, N., Fraser, G.W., et al. 1981, MNRAS, 197, 865
- White, N.E., Mason, K. O., Giommi, P., et al. 1987, MNRAS, 226, 645
- White, N.E., Angelini, L., Ebisawa, K., et al. 1996, ApJ, 463, L83
- Willingale, R., Aschenbach, B., Griffiths, R.G., et al. 2001, A&A, 365, L212
- Winkler, C., Courvoisier, T. J.-L., Di Cocco, G., et al. 2003, A&A, 411, L1
- Woods, P.M., Kaspi, V.M., Thompson, C., et al. 2004, ApJ, 605, 378
- Zhang, S., Collmar, W., Hermesen, W., et al. 2004, A&A, 421, 983